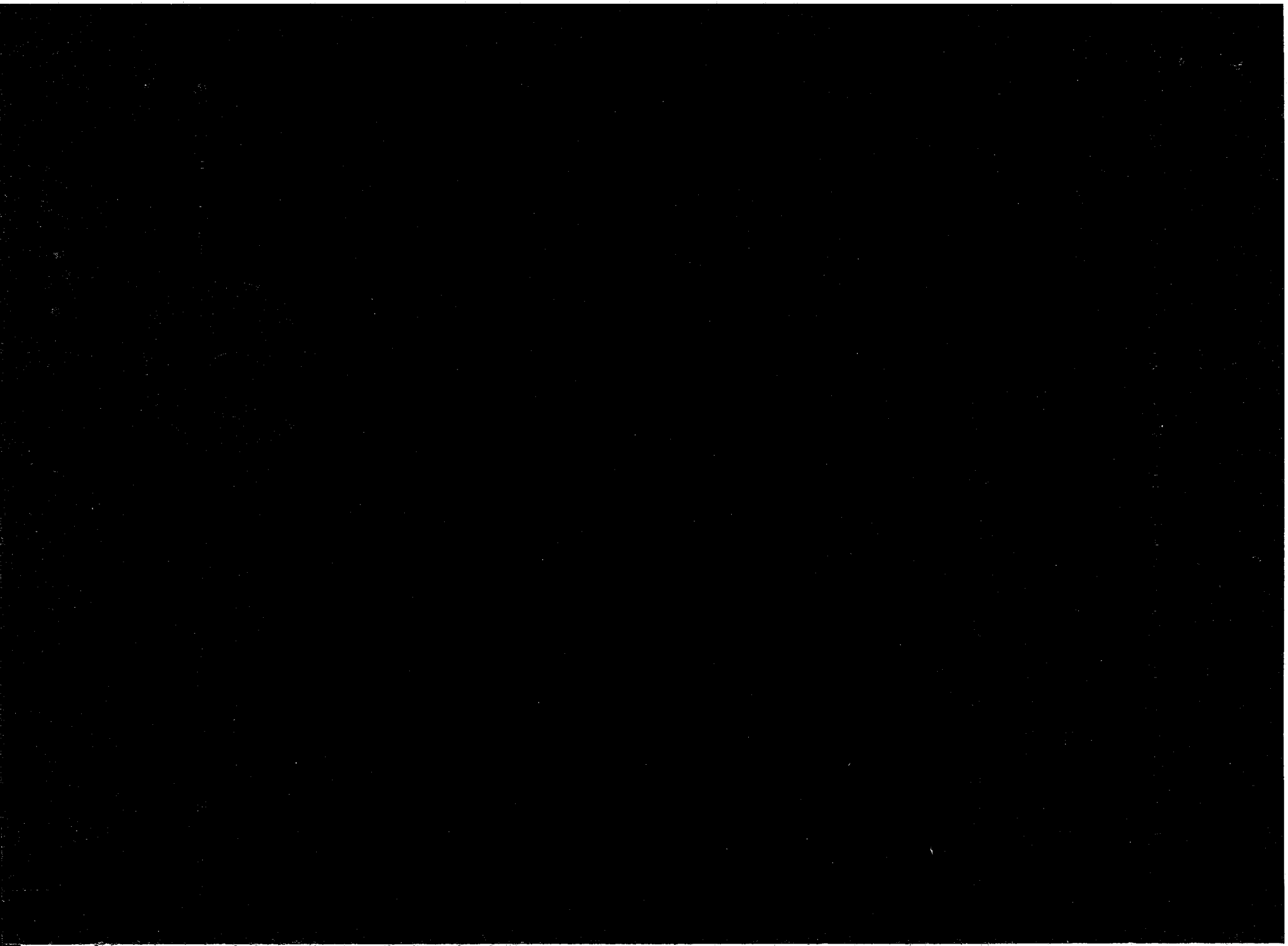

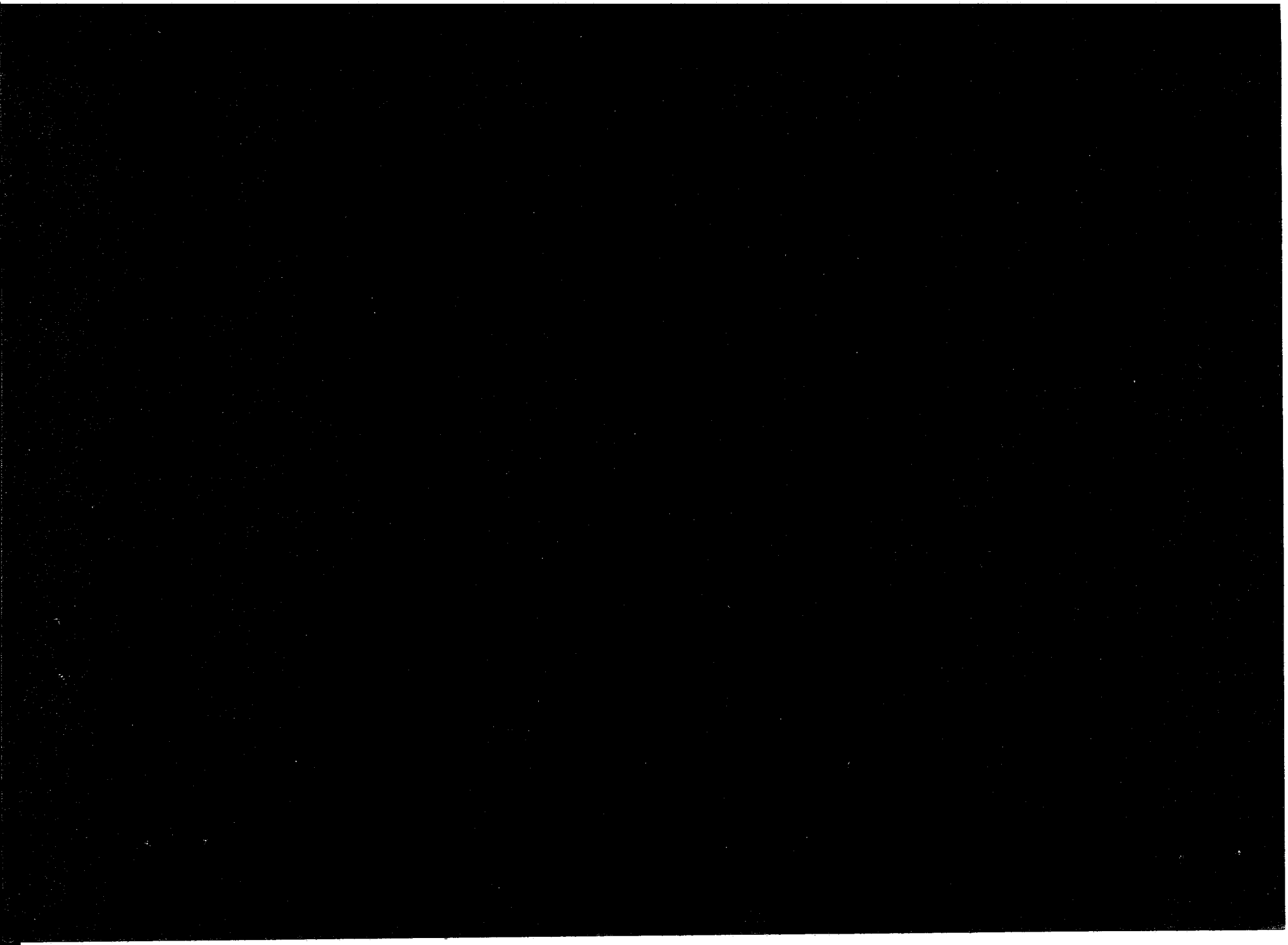

1. Report No. NASA TM X-1999	2. Government Accession No.	3. Recipient's Catalog No.
4. Title and Subtitle STATIC PERFORMANCE OF AN AUXILIARY INLET EJECTOR NOZZLE USING AN AFTERBURNING TURBOJET GAS GENERATOR		5. Report Date April 1970 6. Performing Organization Code
7. Author(s) Richard R. Burley and Ali H. Mansour		8. Performing Organization Report No. E-5459
9. Performing Organization Name and Address Lewis Research Center National Aeronautics and Space Administration Cleveland, Ohio 44135		10. Work Unit No. 720-03 11. Contract or Grant No.
12. Sponsoring Agency Name and Address National Aeronautics and Space Administration Washington, D.C. 20546		13. Type of Report and Period Covered Technical Memorandum 14. Sponsoring Agency Code

15. Supplementary Notes

16. Abstract

Three ejector nozzle configurations which were appropriate for operation at takeoff, transonic acceleration, and supersonic cruise flight conditions were tested over a range of nozzle pressure ratios from 2 to 32. Corrected secondary weight flow was varied from 0.02 to 0.08 and primary exhaust gas temperatures varied between 1651° and 3420° R (917 and 1900 K). The data are presented in terms of pumping characteristics and nozzle efficiency. Typical pressure and temperature profiles along the ejector internal wall surface are also shown.

17. Key Words (Suggested by Author(s))	18. Distribution Statement
Propulsion system Exhaust nozzles	Unclassified - unlimited

19. Security Classif. (of this report)	20. Security Classif. (of this page)	21. No. of Pages	22. Price*
Unclassified	Unclassified	46	$3.00

* For sale by the Clearinghouse for Federal Scientific and Technical Information
Springfield, Virginia 22151

STATIC PERFORMANCE OF AN AUXILIARY INLET EJECTOR NOZZLE USING AN AFTERBURNING TURBOJET GAS GENERATOR

by Richard R. Burley and Ali H. Mansour

Lewis Research Center

SUMMARY

An investigation was conducted in a static altitude facility to determine the performance characteristics of an auxiliary inlet ejector nozzle. The auxiliary inlet doors and the ejector trailing-edge flaps were fixed in positions appropriate for operation at takeoff (flaps closed; doors open), transonic acceleration (flaps closed; doors closed), and supersonic cruise (flaps open; doors closed). Four door configurations were investigated: two simulated single-hinged floating doors positioned at 16° and 20° angles, and two simulated double-hinged floating doors positioned at 8° - 16° and 10° - 20° angles.

The primary jet exhaust was provided by a turbojet engine (J85-GE-13), and the secondary air was furnished by a high-pressure air system. The ratio of corrected secondary flow to primary weight flow varied from 0.02 to 0.08. The primary nozzle area was varied as exhaust gas temperature was varied between 1651° and 3420° R (917 and 1900 K).

For the takeoff configuration, the highest values of nozzle efficiency were of the order of 100 percent and were obtained at low nozzle pressure ratios. It was also found that whenever the tertiary doors were open, the secondary total pressure was nearly equal to ambient pressure p_0. These results were essentially independent of the door configurations investigated.

For the transonic acceleration configuration, increasing the amount of secondary airflow resulted in a marked improvement in nozzle efficiency over the range of nozzle pressure ratios investigated, especially at the lower pressure ratios. A minimum secondary corrected airflow equal to about 6 percent of the primary weight flow was needed for cooling the primary nozzle leaves below 2070° R (1150 K) when the exhaust gas temperature approached 3420° R (1900 K).

For the supersonic cruise configuration with a moderate amount of secondary airflow ($\omega\sqrt{\tau} = 0.06$) and operating near the design pressure ratio, the value of nozzle efficiency was 96 to 99 percent depending on the shroud area ratio. Nozzle efficiency became less sensitive to changes in secondary-to-primary corrected weight flow ratio as diameter ratio decreased. It was also found that secondary airflow was independent of downstream conditions over the range of nozzle pressure ratios investigated.

INTRODUCTION

Airframe installation effects on the performance of several turbojet exhaust nozzle concepts are being evaluated in a flight program at the Lewis Research Center. The nozzle is installed on a nacelle which houses a J-85 turbojet engine and which is mounted under the wing of a modified F-106 aircraft. Prior to flight testing, the internal performance of these nozzles was determined in a static test facility (Propulsion Systems Laboratory Altitude Chamber). The present investigation was conducted in this facility to determine the performance characteristics of an auxiliary inlet ejector nozzle (AIE).

The nozzle system consists of an ejector shroud which has flaps at the shroud exit (trailing-edge flaps) and a series of auxiliary inlet doors located around the periphery of the external skin just ahead of the primary nozzle exit. The basic principles of operation of the nozzle system have been described in the literature (e.g., ref. 1). For this investigation, the auxiliary inlet doors and the trailing-edge flaps were fixed in positions corresponding to operation at takeoff (flaps closed; doors open), transonic acceleration (flaps closed; doors closed), and supersonic cruise (flaps open; doors closed).

The primary jet exhaust was provided by a variable-area-nozzle turbojet engine (J85-GE-13), and the secondary air was furnished by a high-pressure air system. The primary nozzle pressure ratio ranged from about 2 to about 32, and corrected ratio of secondary flow to primary weight flow varied from about 0.02 to 0.08. The turbojet engine nozzle area was varied to give a range of diameter ratios D_S/D_8 (ejector minimum shroud diameter to primary nozzle effective diameter) between 1.18 and 1.52. The engine exhaust gas temperature was varied from about 1651° to 3420° R (917 to 1900 K).

APPARATUS AND PROCEDURE

Installation

A schematic view and a photograph of the research hardware installation in the altitude facility are shown in figures 1 and 2. The turbojet engine was mounted within a nacelle. The entire engine nacelle assembly, including bellmouth, secondary-flow piping, and research ejector nozzle, was mounted from a bedplate freely suspended by four flexure rods. The resultant axial force acting on the engine nacelle assembly during the tests was transmitted to a water-cooled calibrated load cell. A front bulkhead with a labyrinth seal around the inlet section of the nacelle separated the plenum cavity from the altitude chamber to provide a means for adjusting exhaust pressure independent of inlet pressure. Nozzle pressure ratio was varied by changing the cell pressure. A minimal amount of air was admitted to the test section of the altitude chamber through a bypass valve to provide ventilation to adequately keep the test section at an acceptable

temperature level. Exhausters controlled the altitude cell pressure and ejected the gas generator exhaust gases, which were directed into an exhaust duct located immediately downstream of the exit.

Primary and secondary airflows were supplied from separate sources. Primary airflow was supplied to the engine through a bellmouth. Secondary airflow was supplied through a torroidal manifold encompassing the inlet section upstream of the compressor face. The secondary air entered the front of the nacelle to cool both the engine and the primary exhaust nozzle. A rotary valve at the front of the nacelle was used to adjust secondary airflow (see ref. 2 for details).

A J85-GE-13 engine (SN 243775) was used as the gas generator. It is an afterburning turbojet engine incorporating an eight-stage, axial-flow compressor, a two-stage turbine, and a variable-area primary exhaust nozzle. The engine has a dry mass of 570 pounds (258.5 kg), a rated airflow of 44 pounds per second (19.96 kg/sec), and a rated sea-level static thrust of 2720 pounds force (12.1 kN) at military power and 4080 pounds force (18.15 kN) at maximum afterburning. The engine had been calibrated previously in the same facility (ref. 3).

Primary Nozzle

The variable-area primary exhaust nozzle closely approximates a circular geometry. As the exit area is varied, the nozzle translates longitudinally and a corresponding change occurs in the nozzle convergence angle (see fig. 3). The overlapping primary leaves translate on a roller-track-cage arrangement into a nozzle-housing ring. The nozzle-housing ring has a series of 24 rectangular holes (see fig. 4) located circumferentially around the ring. A secondary-flow deflector forced secondary cooling air under the nozzle-housing ring and over the primary leaves.

Auxiliary Inlet Ejectors

Details of the ejectors and auxiliary inlet doors are presented in figures 4 and 5, and shown in figures 6 to 8. The ejectors have a maximum diameter of 25 inches (63.5 cm). The takeoff and transonic acceleration ejector had the trailing-edge flaps fixed in the closed position, resulting in an exit diameter of 18.19 inches (46.2 cm) and a boattail angle of 15°. When this ejector is used with open auxiliary inlet doors, it is referred to as the takeoff configuration; with the doors closed, it is referred to as the transonic acceleration configuration. The supersonic cruise ejector had the trailing-edge flaps fixed in the wide-open position, providing a cylindrical outer contour and a divergence angle of 9° on the inner wall of the shroud. The variations in diameter ratio

D_S/D_8 and spacing ratios L_e/D_8 and L/D_8 with primary nozzle effective area A_8 are shown in figure 9(a). Primary nozzle effective area ranged between 108 and 187 square inches (700 and 1205 cm^2) for the takeoff and transonic acceleration ejector, and between 108 and 164 square inches (700 and 1060 cm^2) for the supersonic cruise ejector. The largest area tested with the supersonic cruise ejector was limited to 164 square inches (1060 cm^2) to ensure that the primary nozzle leaf temperature remained within the safe operating range below 2070° R (1150 K).

The auxiliary inlet door sections were removable and four sets of fixed-open doors were used; two sets simulated single-hinged floating doors positioned at 16° and 20° angles, and two sets simulated double-hinged floating doors positioned at 8° - 16° and 10° - 20° angles. The doors positioned at 20° or 10° - 20° resulted in an open area A_{AID} of 163 square inches (1052 cm^2); positioning the doors at 16° or 8° - 16° resulted in A_{AID} = 136.9 square inches (883.2 cm^2).

The purpose of the doors is to allow tertiary air to enter the ejector and provide an aerodynamically smaller ejector exit area, which helps keep the primary jet properly expanded. The difference between the actual ejector exit area and the ejector exit area to properly expand the primary flow is referred to as the overexpansion area. The variation in overexpansion area with nozzle pressure ratio is presented in figure 9(b) for the three diameter ratios for the takeoff configuration. With diameter ratios of 1.33 and 1.52, an overexpansion area exists over the entire range of nozzle pressure ratios. For the diameter ratio of 1.18, an overexpansion area exists up to a pressure ratio of about 5.

Also shown in figure 9(b) are the auxiliary inlet door open areas for the doors positioned at 16° or 8° - 16° and 20° or 10° - 20°. When the doors are wide open (20° or 10° - 20°), the open area is greater than the overexpansion area for each of the three diameter ratios over the entire range of nozzle pressure ratios. When the doors are positioned at 16° or 8° - 16°, the open area is greater than the overexpansion area for the diameter ratios of 1.18 and 1.33 over the entire range of nozzle pressure ratios. For the diameter ratio of 1.52, the open area is greater than the overexpansion area for nozzle pressure ratios greater than about 3.2.

Instrumentation

Location and details of the measuring stations of the engine-nacelle installation and ejector hardware are shown in figures 1 and 10 to 12. All thermocouples were Chromel-Alumel, and those in the secondary passage had radiation shields. Skin temperatures were measured with the juncture of the thermocouple embedded in the skin, flush with the hot surface side.

The engine was instrumented to record and monitor the engine operating parameters

at the stations indicated in figure 1. The instrumentation was the same as that of reference 3 except at the compressor face (station 2). Average total pressure at station 2 was obtained from 15 area-weighted probes located in three hollow deicing struts.

Two standard ASME sharp-edged orifices were used to measure secondary airflow. Total pressure and temperature of the secondary airflow were measured at the locations indicated in figure 10.

The location of the instrumentation for the auxiliary inlet doors and the ejectors is shown in figures 11 and 12. Static-pressure taps and skin thermocouples were located along the internal surface of the auxiliary inlet doors and the ejectors. Static-pressure taps also were located on the external surface at the exit of the ejector. They were used to determine ambient pressure p_0.

Procedure

Performance characteristics of the ejectors were investigated at secondary-to-primary corrected weight flow ratios $\omega\sqrt{\tau}$ from 0.02 to 0.08 over a range of nozzle total-pressure ratios P_8/p_0 for several values of engine-power setting. The takeoff and transonic acceleration ejector was tested over a range of P_8/p_0 values from about 2 to 6 and three or four engine-power settings (four engine-power settings with doors closed). The supersonic cruise ejector was investigated over a range of P_8/p_0 values from 5 to 33 and four power settings. The resulting values of primary nozzle effective area A_8 and corresponding exhaust gas total temperature T_8 for the ejectors are presented in the following table:

Ejector tested	Primary nozzle effective area, A_8		Exhaust gas total temperature, T_8	
	$in.^2$	cm^2	^oR	K
Takeoff and transonic acceleration ejector	108	700	1651	917
	146	940	2547	1415
	159	[a]1026	2970	[a]1650
	187	1205	3420	1900
Supersonic cruise ejector	108	700	1651	917
	139	895	2439	1355
	152	980	2781	1545
	164	1060	3105	1725

[a]Only with doors closed.

Conditions in the plenum cavity of the test facility were maintained relatively constant at a total temperature of 535° R (297 K) and at total pressures of 0.638 atmosphere for the takeoff and transonic acceleration ejector and 1 atmosphere for the supersonic cruise ejector. For a constant value of A_8, the value of P_8/p_0 was varied by changing cell pressure p_0; A_8 was varied by changes in engine-power setting. At each power setting, the general procedure was first to set a value for cell pressure and then to record data at values of $\omega\sqrt{\tau}$ between 0.02 and 0.08. The procedure was repeated for several values of cell pressure to achieve the desired range of P_8/p_0 values. Then the entire procedure was repeated for several engine-power settings.

Pressure in the annular passage just upstream of the secondary-flow valve was maintained at the same value as compressor-face pressure and the secondary-flow-valve area was modulated to set various secondary flows. Several ejector-skin and primary-leaf temperatures were monitored continuously during the test to ensure safe operating conditions.

Data Reduction

To determine ejector nozzle performance, conditions at the exit of the primary exhaust nozzle (station 8) must be known. Total temperature T_8, total pressure P_8, and effective area A_8 were obtained by using the values of engine airflow, engine and afterburner fuel flows, the total pressure and temperature at the turbine discharge (station 5), along with afterburner temperature rise and pressure drop calibration results from reference 3. Total weight flow through the primary nozzle W_{g8} is the sum of engine airflow and engine-plus-afterburner fuel flows. Engine airflow was determined from static pressures in the 14-inch- (35.56-cm-) diameter venturi throat (station 1, fig. 1), a flow coefficient, and total pressures and temperatures ahead of the bellmouth. Fuel flows were obtained from calibrated flowmeters.

Ejector gross thrust F_G is defined as the sum of the gross thrusts of the primary and secondary streams plus net thrust of the tertiary stream; that is, it is the total momentum of the internal flow at ejector exit minus the total momentum of the tertiary air at the entrance to the auxiliary inlet doors. The axial force transmitted to the load cell was composed of the following: (1) total momentum of the internal flow at the ejector exit, (2) total momentum of tertiary air at the entrance to the auxiliary inlet doors, (3) total inlet momentum of the primary stream, and (4) nacelle-bellmouth tare force. The ejector gross thrust was obtained by subtracting the tare force and adding the total inlet momentum of the primary stream to the load-cell measurement. The ideal thrust of the primary F_{ip} and secondary F_{is} streams was calculated from the measured primary and secondary mass flows, with isentropic expansion assumed from the respec-

tive values of total pressure and temperature to ambient pressure. Ideal thrust of the secondary stream was set to zero when secondary total pressure was less than ambient ($P_s < p_0$).

Two thrust parameters are presented: (1) nozzle efficiency (nozzle gross thrust divided by the sum of the ideal primary and secondary thrusts), and (2) nozzle gross thrust coefficient (nozzle gross thrust divided by ideal primary thrust). These two parameters, along with the secondary-to-primary total-pressure ratio and the nozzle pressure ratio were plotted for each ejector initially as a function of secondary-to-primary corrected weight flow ratio at each value of A_8. Then values of each of these parameters were interpolated or extrapolated to obtain the parameters at secondary-to-primary corrected weight flow ratios of 0.02, 0.04, 0.06, and 0.08. Thus, the symbols shown on figures 13 to 21 do not necessarily represent actual data points. However, the symbols used for the pressure and temperature distributions of figures 22 to 24 do represent actual data points. The symbols used in figure 25 also represent actual data points.

RESULTS AND DISCUSSION

The pumping and thrust characteristics of the ejectors are presented. Then typical pressure and temperature profiles along the internal surface of the ejectors are shown. Finally, the secondary-flow characteristics of total-pressure loss and circumferential temperature gradients are given.

Pumping and Thrust Characteristics

Pumping characteristics P_s/P_8, thrust efficiency $F_G/(F_{ip} + F_{is})$, and nozzle gross thrust coefficient F_G/F_{ip} are presented in figures 13 to 21. (Ideal secondary thrust is set to zero when secondary stream total pressure is less than ambient $P_s < p_0$ and is noted by the tailed symbols.) Each of the three parameters is plotted as a function of primary nozzle total-pressure ratio at secondary-to-primary corrected weight flow ratios of 0.02, 0.04, 0.06, and 0.08 for several diameter ratios. (The values of secondary-to-primary corrected weight flow ratios were obtained from cross plots so the symbols do not necessarily represent actual data points.) Three values of the diameter ratio are presented for the takeoff configuration and four are shown for the transonic acceleration and supersonic cruise configurations.

Takeoff configuration. - Pumping characteristics of the takeoff configuration are presented in figures 13(a) to (d). For a given diameter ratio, the secondary total pressure required to pump a given secondary flow decreased as nozzle total-pressure ratio

was increased. Thus, pumping performance improved considerably with increasing nozzle total-pressure ratio. A further small improvement in pumping performance was obtained by increasing the diameter ratio.

Whenever the tertiary doors are open, the secondary total pressure is nearly equal to ambient pressure p_0. A comparison of P_s/P_8 and p_0/P_8 over a range of nozzle pressure ratios P_8/p_0 is given in the following table (from fig. 13(a) at $\omega\sqrt{\tau} = 0.04$):

Nozzle pressure ratio, P_8/p_0	Secondary-to-primary total-pressure ratio, P_s/P_8	Static to primary-total-pressure ratio, p_0/P_8
2.35	0.415	0.426
3.25	.30	.308
5.75	.19	.174

Over the range of nozzle pressure ratios, the corresponding value of P_s closely follows p_0.

That the values of P_s and p_0 are closely related also can be inferred from pumping performance figures by noting the tailed symbols (tailed symbols indicate $P_s < p_0$). For example, as more corrected flow is pumped at a nozzle pressure ratio of 3.25 (fig. 13(a-1)), the value of P_s goes from less than p_0 for $\omega\sqrt{\tau}$ of 0.02 and 0.04 to greater than p_0 for $\omega\sqrt{\tau}$ of 0.06 and 0.08. Thus, $P_s = p_0$ between $\omega\sqrt{\tau}$ of 0.04 and 0.06.

Figures 14 and 15 show the thrust characteristics. In general, as the nozzle total-pressure ratio was increased from a value of about 2, nozzle efficiency first increased and then decreased as pressure ratio was further increased. The initial increase in efficiency suggests that a substantial amount of tertiary air was drawn through the auxiliary inlet doors by the primary and secondary streams at low pressure ratios. At pressure ratios less than 3, values of nozzle efficiency of the order of 100 percent were obtained. In the definition of nozzle efficiency, the actual net thrust contribution of the tertiary stream was included in the numerator, but its ideal gross thrust contribution was neglected in the denominator. Consequently, efficiencies greater than 100 percent are possible.

Both pumping and thrust performance were essentially independent of the four door configurations investigated. There is not a large difference in auxiliary inlet door open area between the doors positioned at 16° or 8° - 16° (A_{AID} = 136.9 in.^{2} (883.2 cm^2))

and the doors positioned at 20° or 10° - 20° (A_{AID} = 163 in.^{2} (1052 cm^2)). Also, the open area generally is substantially greater than the overexpansion area (see fig. 9(b)).

Transonic acceleration configuration. - The pumping characteristics of the transonic acceleration configuration are presented in figure 16. Secondary-to-primary total-pressure ratio required to pump a given amount of secondary flow decreased almost linearly to a minimum value as nozzle total-pressure ratio was increased. The nozzle total-pressure ratio at which the minimum value of secondary-to-primary total-pressure ratio occurs corresponds to primary flow attachment to the shroud and is referred to as the breakoff value. Further increases in pressure ratio had no effect on the value of secondary-to-primary total-pressure ratio. At pressure ratios greater than the breakoff value, secondary total-pressure ratio P_s/P_8 increased as the diameter ratio D_s/D_8 was decreased. A minimum secondary corrected airflow equal to about 6 percent of primary weight flow was needed to cool the primary nozzle (i.e., maintain nozzle skin temperature less than 2070° R (1150 K)) when the primary gas temperature approached 3420° R (1900 K).

Thrust characteristics are shown in figures 17 and 18. In general, as the nozzle total-pressure ratio was increased from a value of about 2, nozzle efficiency first decreased as the primary flow became effectively attached to the shroud and then increased as the pressure ratio was increased toward the design pressure ratio. The extent of the initial decrease in efficiency depends on the amount of secondary flow. Increasing the amount of secondary flow resulted in a marked improvement in thrust efficiency especially at the lower pressure ratios (<3). However, the nozzle efficiency still showed a sharp dip at an initial nozzle pressure ratio between 2 and 3. This characteristic is different from that observed for the takeoff configuration, where open doors could furnish tertiary flow so that nozzle efficiency initially increased as pressure ratio was increased from a value of 2. Although moderate amounts of secondary flow achieve a performance improvement, the use of tertiary air further improves performance over a limited range of nozzle total-pressure ratios.

Supersonic cruise configuration. - The pumping characteristics of the supersonic cruise configuration are presented in figure 19, and the thrust characteristics are shown in figures 20 and 21. In general, the shapes of the curves are similar to those of the transonic configuration for values of nozzle total-pressure ratio greater than breakoff. Thus, secondary airflow was independent of downstream conditions over the entire range of nozzle pressure ratios investigated. Nozzle efficiency increased as nozzle pressure ratio was increased and reached a peak value near the design pressure ratio. (The design pressure ratio is defined as that pressure ratio which would result from one-dimensional expansion of the flow from the primary nozzle area to the ejector exit area.) Near the design pressure ratio and with a moderate amount of secondary airflow ($\omega\sqrt{\tau}$ = 0.06), the value of nozzle efficiency was 96 to 99 percent depending on the diam-

eter ratio. The peak efficiency of 99 percent was obtained at a diameter ratio $D_S/D_8 = 1.52$. As the diameter ratio decreased, the peak efficiency first decreased to a value of 96.3 percent at $D_S/D_8 = 1.30$, and then increased to 97.5 percent with a further decrease in D_S/D_8 to 1.25. No reason is apparent for this trend. Nozzle efficiency became less sensitive to variations in secondary weight flow as the diameter ratio was increased.

Wall Pressure and Temperature Profiles

Typical dimensionless pressure and temperature profiles along the internal surface of the ejectors are presented in figures 22 to 24 for several diameter ratios. The wall pressures and temperatures are ratioed to the primary exhaust gas total pressure and total temperature, respectively. Axial distance x is measured from the exit plane of the primary nozzle and was ratioed to primary nozzle effective diameter. In general, negative values are associated with measurements made on the door surfaces (see figs. 11 and 12). For the supersonic cruise configuration, the profiles also are presented as a function of area ratio A/A_8, and the data are shown for all four values of D_S/D_8 investigated. The ambient static pressure level is indicated for each condition by a dashed line at the right of the figure.

At low nozzle total-pressure ratios, the wall static pressures are near ambient for the takeoff configuration (figs. 22(a-1) and 22(b-1)) but are moderately lower than ambient for the transonic acceleration configuration especially near the primary nozzle exit (figs. 23(a) and (c)). As the pressure ratio is increased, the primary stream expands and effectively attaches to the ejector wall, thus restricting the secondary flow (and tertiary flow for the takeoff configuration). At this condition, the wall static pressures are considerably below ambient throughout most of the ejector. For the transonic acceleration configuration, the wall attachment occurs at a nozzle pressure ratio between 2.96 and 3.99 for a diameter ratio of 1.52 (fig. 23(a)) and between 2 and 2.75 for a diameter ratio of 1.18 (fig. 23(c)). For the supersonic cruise configuration, it occurs below the lowest pressure ratio tested; that is, less than 5.95 for a diameter ratio of 1.52 (fig. 24(a)) and less than 5.49 for a diameter ratio of 1.25 (fig. 24(c)). For the takeoff configuration, the wall attachment appears to occur at a pressure ratio between 3.65 and 5.48 for the diameter ratio of 1.52 (fig. 22(a-1)) and between 2.5 and 2.9 for the diameter ratio of 1.18 (fig. 22(a-3)). As nozzle pressure ratio is increased further, primary separation and recompression occur downstream of the attachment point, returning the pressure to ambient at the exit of the ejector. The static-pressure profile upstream of the recompression becomes independent of increases in nozzle pressure ratio. The location of the recompression moves downstream as the nozzle pressure ratio is increased

until a value is reached where the recompression to p_0 is no longer present inside the ejector. Then the ejector is flowing full but slightly overexpanded. Any further increases in nozzle pressure ratio do not affect the internal ejector characteristics.

The maximum skin temperatures for the takeoff and the transonic acceleration configurations occur near the midpoint of the ejector over the range of power settings investigated. For the supersonic cruise configuration, the maximum skin temperatures occur near the midpoint of the ejector for military power setting and near the ejector exit for the highest power setting.

Secondary-Flow Characteristics

Total-pressure loss through the secondary-flow passage as a function of secondary-to-primary corrected weight flow ratio is presented in figure 25 for the transonic acceleration configuration and the takeoff configuration with the 10° - 20° open doors. The loss is not influenced by nozzle pressure ratio as long as the nozzle pressure ratio values are greater than breakoff. The transonic configuration was tested over a range of nozzle pressure ratio values that were both greater than and less than breakoff. The total-pressure loss for this configuration is shown in figures 25(a-1) and (a-2) for nozzle pressure ratio values greater than and less than breakoff, respectively. The pressure loss characteristics of the supersonic cruise configuration are similar to those of figure 25(a) since all the nozzle pressure ratio values investigated were greater than breakoff. For the takeoff configuration, no breakoff values were encountered. The total-pressure loss for this configuration with the 10° - 20° open doors is shown in figure 25(b).

The circumferential variation in total temperature of the secondary airflow measured at station 200.35 inches (508.89 cm) is shown in table I. Temperatures were measured at four circumferential locations, 0°, 90°, 180°, and 270° (see fig. 10). A substantial gradient exists especially at small values of secondary-to-primary corrected weight flow ratios ($\omega\sqrt{\tau} \sim 0.03$) and afterburning diameter ratios ($D_S/D_8 < 1.5$). For the transonic acceleration configuration at $D_S/D_8 = 1.28$ and $\omega\sqrt{\tau} = 0.0276$, a temperature gradient of 211° R (117 K) was measured. The high temperature (1069° R, 594 K) was measured at the 90° location and the low temperature (858° R, 477 K) was measured at the 270° location. For the takeoff configuration at $D_S/D_8 = 1.33$ and $\omega\sqrt{\tau} = 0.025$, a temperature gradient of 187° R (104 K) was measured. The high temperature (1021° R, 567 K) was measured at 0° and the low temperature (834° R, 463 K) was measured at 270°.

No significant circumferential variation in total pressure was measured at station 200.35 inches (508.89 cm).

SUMMARY OF RESULTS

An investigation of the thrust and pumping performance of three ejector configurations representative of operation at flight conditions of takeoff, transonic acceleration, and supersonic cruise has been conducted in a static altitude facility. Data were obtained at corrected secondary-to-primary weight flow ratios between 0.02 and 0.08 over a range of exhaust nozzle pressure ratios from 2 to 33, ejector exit to primary nozzle diameter ratios between 1.18 and 1.52, and primary exhaust gas temperatures between 1651° and 3420° R (917 and 1900 K). Results of the investigation may be summarized as follows:

Takeoff configuration:

1. Whenever the tertiary doors were open, the secondary total pressure was nearly equal to ambient pressure p_0.

2. Generally, the highest values of nozzle efficiency, of the order of 100 percent, were obtained at low nozzle pressure ratios (<3).

3. Both pumping and thrust performance were essentially independent of the four door configurations investigated.

Transonic configuration:

1. Increasing the amount of secondary airflow resulted in a marked improvement in nozzle efficiency especially at the lower pressure ratios (<3) and higher shroud area ratios ($A_s/A_8 > 1.77$).

2. A minimum secondary corrected airflow equal to about 6 percent of the primary weight flow was needed for cooling the primary nozzle leaves below 2070° R (1150 K). when the exhaust gas temperature approached 3420° R (1900 K).

Supersonic cruise configuration:

1. With a moderate amount of secondary airflow ($\omega\sqrt{\tau} = 0.06$) and near the design pressure ratio, the value of nozzle efficiency was 96 to 99 percent, depending on the diameter ratio D_s/D_8. Nozzle efficiency became less sensitive to changes in secondary-to-primary corrected weight flow ratio as diameter ratio decreased.

2. Secondary airflow was independent of downstream conditions over the range of nozzle pressure ratios investigated for this configuration (5.5 to 32).

Lewis Research Center,
National Aeronautics and Space Administration,
Cleveland, Ohio, January 9, 1970,
720-03.

APPENDIX - SYMBOLS

A	area (cold), in.^{2} (cm^2)
A_{AID}	auxiliary inlet door open area, in.^{2} (cm^2)
A_{OE}	overexpansion area, in.^{2} (cm^2)
A_8	primary nozzle exit effective flow area, in.^{2} (cm^2)
a	axial distance of instrumentation from compressor face (compressor face arbitrarily assigned station 100 in. (250 cm))
B	axial length (see fig. 5), in. (cm)
D	diameter (cold), in. (cm)
D_8	primary nozzle exit effective diameter, in. (cm)
D_S	ejector minimum shroud diameter, in. (cm)
F	thrust, lbf (kN)
F_G	measured ejector internal gross thrust, lbf (kN)
L	axial distance from primary nozzle exit to secondary throat, in. (cm)
LD_8	axial location of primary nozzle exit from compressor face, in. (cm)
L_e	axial distance from primary nozzle to ejector exit, in. (cm)
l	auxiliary inlet door length (see fig. 5), in. (cm)
P	absolute total pressure, psia (kN/m^2)
P'_s	secondary absolute total pressure measured at station 181 in. (460 cm), psia (kN/m^2)
p	absolute static pressure, lb/in.^{2} (kN/m^2)
R	axial length (see fig. 5), in. (cm)
r	radius, in. (cm)
r_β	boattail juncture radius, in. (cm)
S	auxiliary inlet door dimension (see fig. 5), in. (cm)
T	total temperature, $^\circ$R (K)
t	static temperature, $^\circ$R (K)
x	axial distance from primary nozzle (see figs. 11 and 12), in. (cm)
α	angle of auxiliary inlet door from horizontal (see fig. 5)
γ	primary nozzle convergence angle (see fig. 3)
τ	ratio of secondary to primary total temperatures
ω	ratio of secondary to primary weight flows
$\omega\sqrt{\tau}$	secondary-to-primary corrected weight flow ratio

Subscripts:

d	downstream
ej	ejector wall
ip	one-dimensional isentropic expansion of primary flow

is	one-dimensional isentropic expansion of secondary flow
n	nozzle maximum diameter
s	secondary stream or ejector throat
u	upstream
0	ambient in altitude cell
8	primary nozzle exit
9	ejector shroud exit

REFERENCES

1. Migdal, David; and Horgan, John T.: Thrust Nozzles for Supersonic Transport Aircraft. J. Eng. Power, vol. 86, no. 2, Apr. 1964, pp. 97-104.

2. Samanich, Nick E.; and Huntley, Sidney C.: Thrust and Pumping Characteristics of Cylindrical Ejectors Using Afterburning Turbojet Gas Generator. NASA TM X-52565, 1969.

3. Antl, Robert J.; and Burley, Richard R.: Steady-State Airflow and Afterburning Performance Characteristics of Four J85-GE-13 Turbojet Engines. NASA TM X-1742, 1969.

TABLE I. - CIRCUMFERENTIAL TEMPERATURE GRADIENTS IN SECONDARY-FLOW PASSAGE

Configuration	Ratio of ejector minimum shroud diameter to primary nozzle exit effective diameter, D_s/D_8	Nozzle total-pressure ratio, P_8/p_o	Secondary-to-primary corrected weight flow ratio, $\omega\sqrt{\tau}$	Circumferential location (see fig. 10)							
				0^o		90^o		180^o		270^o	
				Total temperature at station 200.35 inches (508.89 cm)							
				^oR	K	^oR	K	^oR	K	^oR	K
Transonic acceleration	1.52	2.2	0.0758	854	474	805	445	808	449	720	400
		2.2	.0524	883	491	906	503	906	503	820	456
		2.2	.030	995	553	1094	608	993	552	958	532
		6.5	.0753	771	428	772	429	777	432	707	393
		6.5	.0595	826	459	844	469	818	454	772	429
		6.5	.0294	992	551	987	548	1073	596	909	505
	1.28	2.1	0.0694	808	449	766	426	805	447	683	379
		2.1	.050	861	478	884	491	871	484	713	396
		2.1	.0275	1005	558	1061	589	1037	576	852	473
		6.4	.071	828	460	772	429	809	449	683	379
		6.4	.0436	854	474	908	504	923	513	735	408
		6.4	.0276	968	538	1069	594	1039	577	858	477
Takeoff: 10^o - 20^o doors	1.52	2.4	0.0797	811	451	772	429	786	437	697	387
		2.4	.0637	868	482	819	455	833	463	719	399
		2.4	.0281	1018	565	1047	582	993	552	919	511
	1.33	2.2	0.0724	806	448	723	402	773	429	673	374
		2.2	.0527	928	516	848	471	854	474	714	397
		2.2	.025	1021	567	970	539	945	525	834	463

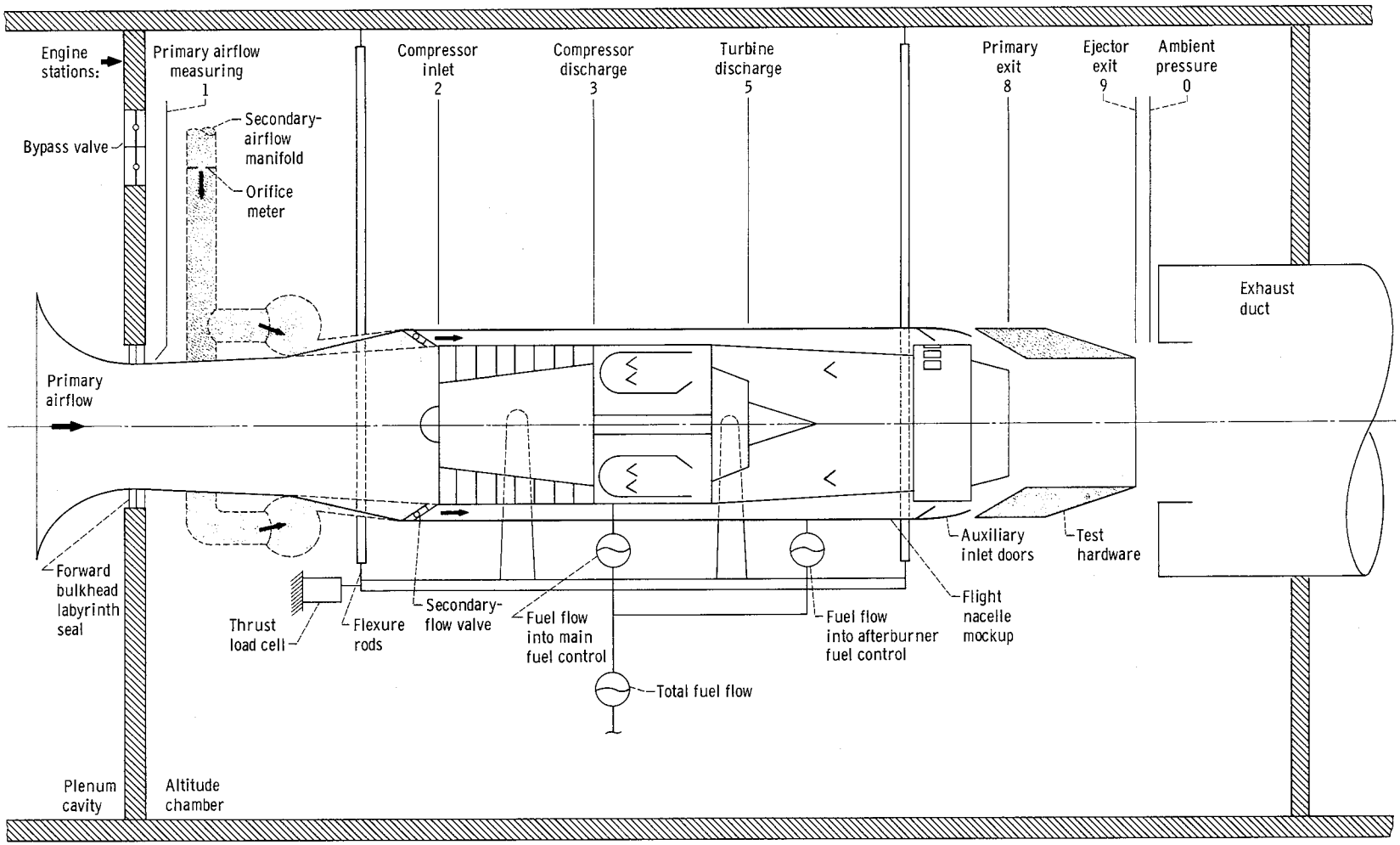

Figure 1. - Schematic of test installation.

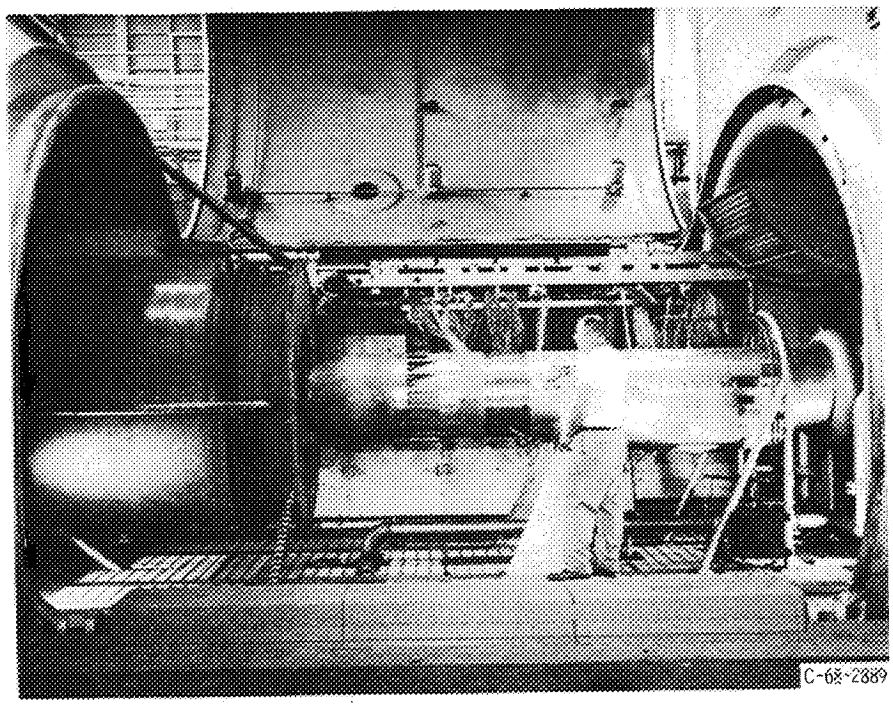

Figure 2. - Test hardware in altitude facility (20° open doors installed).

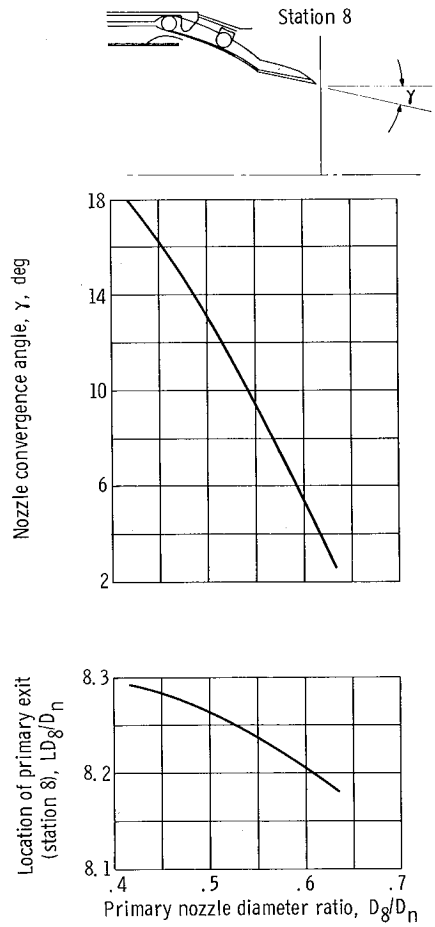

Figure 3. - Primary nozzle dimensional characteristics.

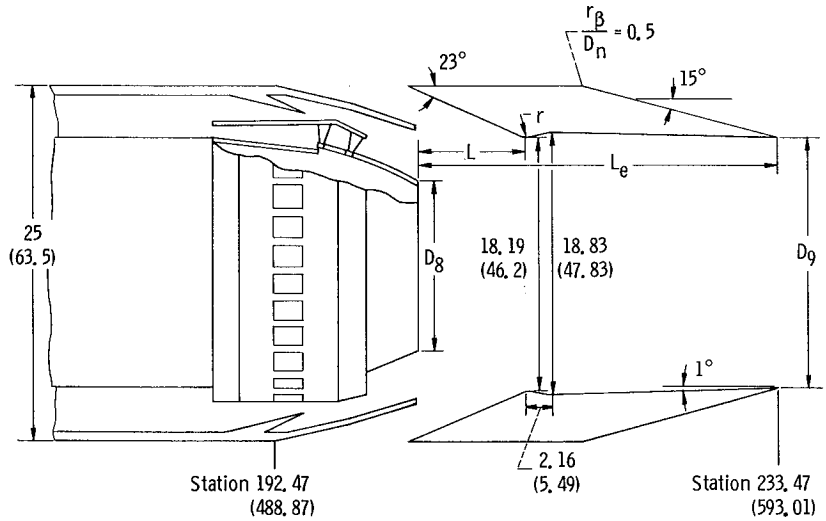

(a) Takeoff and transonic acceleration ejector.

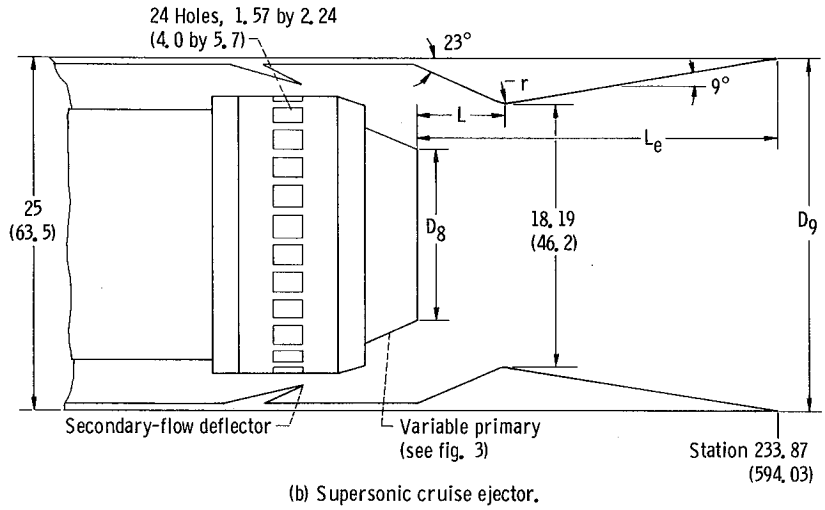

(b) Supersonic cruise ejector.

Trailing-edge flaps	D_9		$L_e - L$		r	
	in.	cm	in.	cm	in.	cm
Open	25	63.5	20.79	52.81	2.89	7.34
Closed	18.19	46.2	20.39	51.79	2.89	7.34

Figure 4. - Dimensional characteristics of ejector nozzles. (All dimensions are in inches (cm).)

Station 192.47
(488.87)

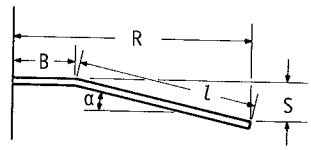

(a) Single-hinged doors.

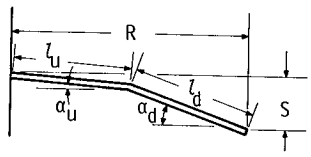

(b) Double-hinged doors.

α, deg	l		S		R		B		A_{AID}	
	in.	cm	in.	cm	in.	cm	in.	cm	$in.^2$	cm^2
16	9.03	22.94	2.49	6.32	11.71	29.74	3.03	7.70	136.9	883.2
20	9.05	22.98	3.09	7.85	11.55	29.34	3.05	7.74	163	1052

α_u, deg	α_d, deg	l_u, l_d		S		R			A_{AID}	
		in.	cm	in.	cm	in.	cm		in.	cm
8	16	6	15.24	2.49	6.32	11.71	29.74		136.9	883.2
10	20	6	15.24	3.09	7.85	11.55	29.34		163	1052

Figure 5. - Dimensional characteristics of auxiliary inlet doors. Door width, 3.87 inches (9.83 cm).

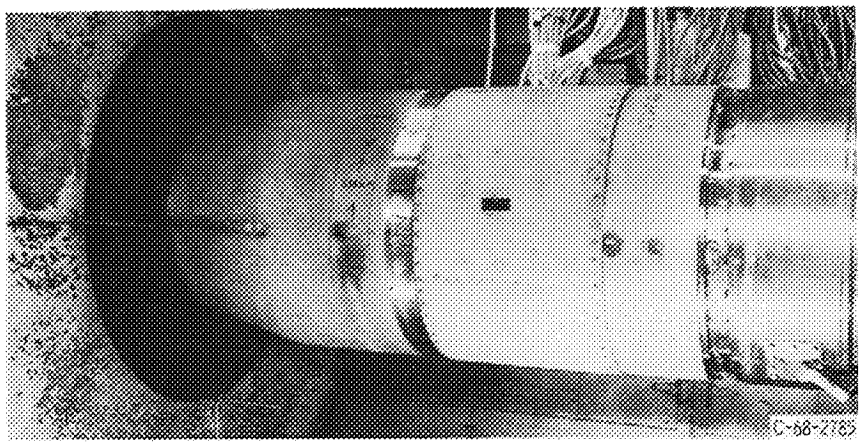

Figure 6. - Transonic ejector configuration (flaps closed; doors closed).

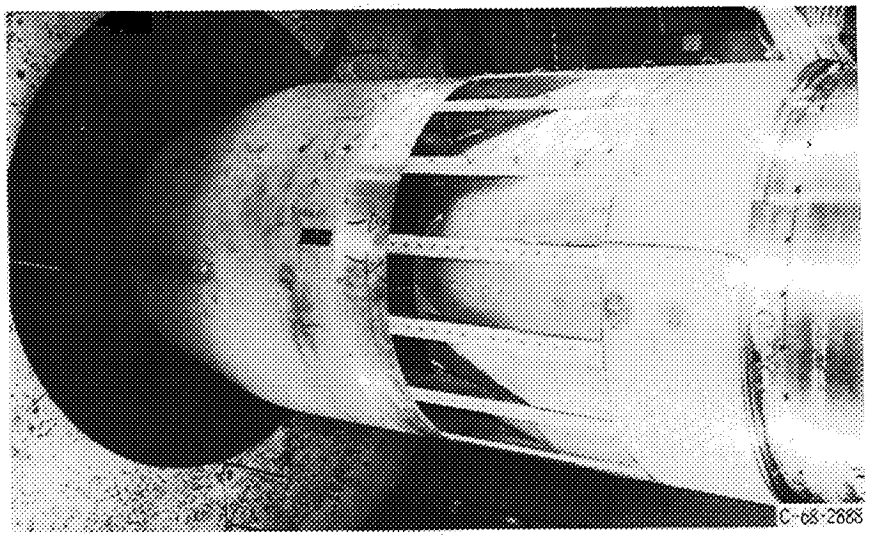

(a) With 20° open doors.

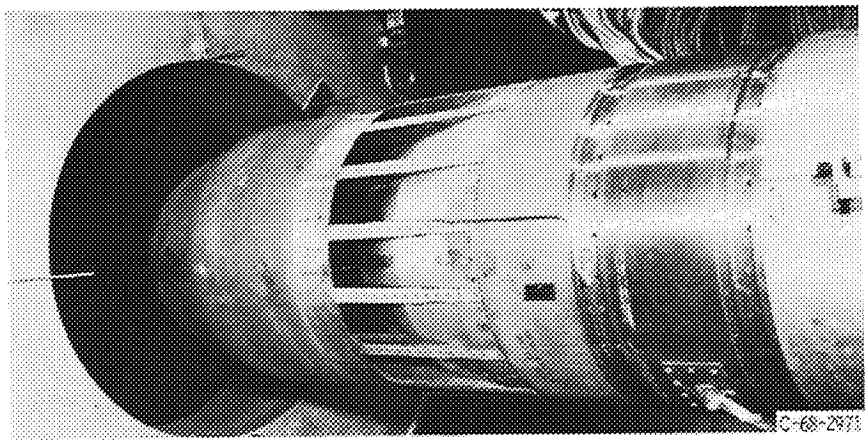

(b) With 10°-20° open doors.

Figure 7. - Takeoff ejector configuration (flaps closed).

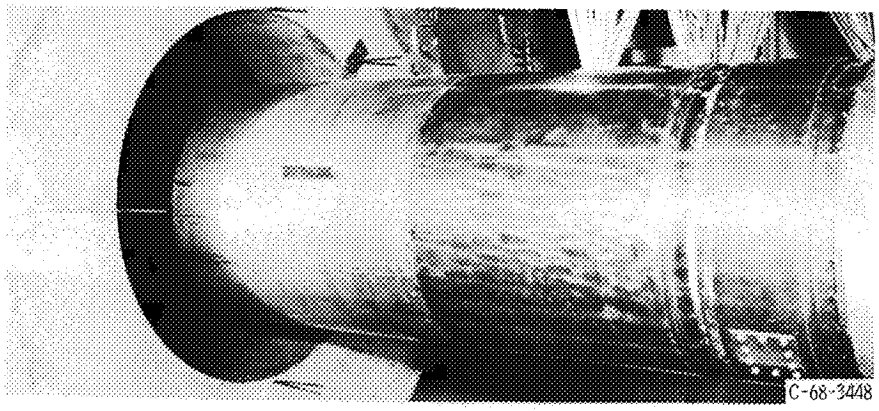

Figure 8. - Supersonic cruise ejector configuration (flaps open; doors closed).

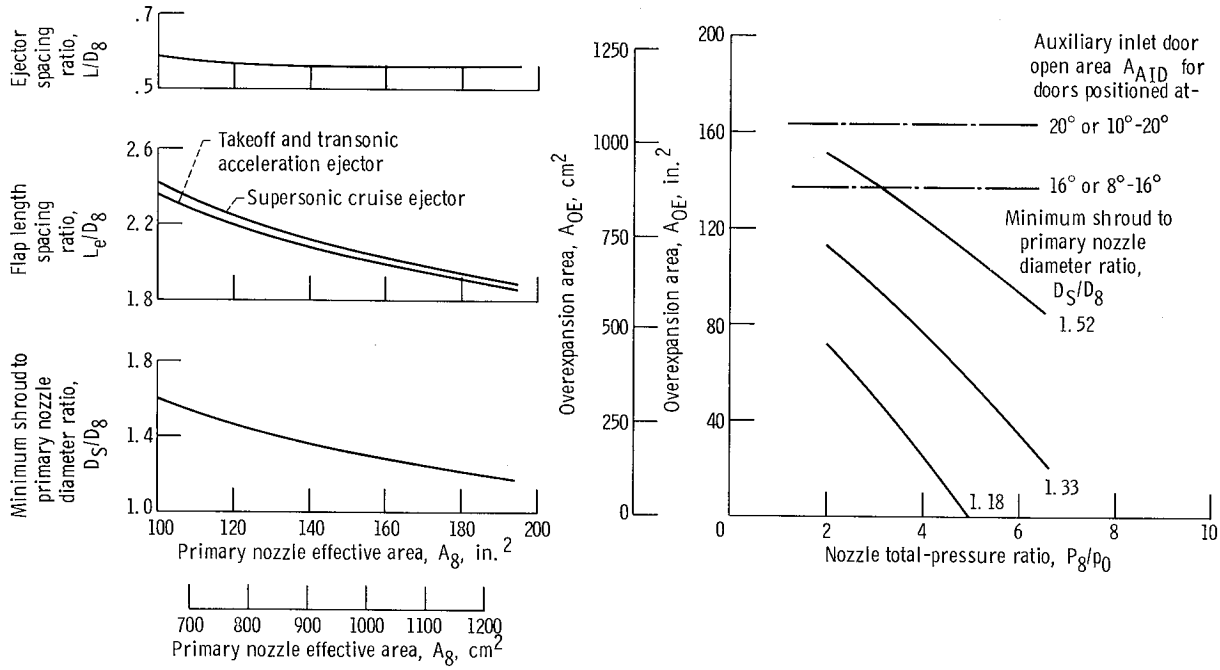

(a) Ejector diameter and spacing ratios.

(b) Overexpansion area.

Figure 9. - Geometric characteristics of ejectors.

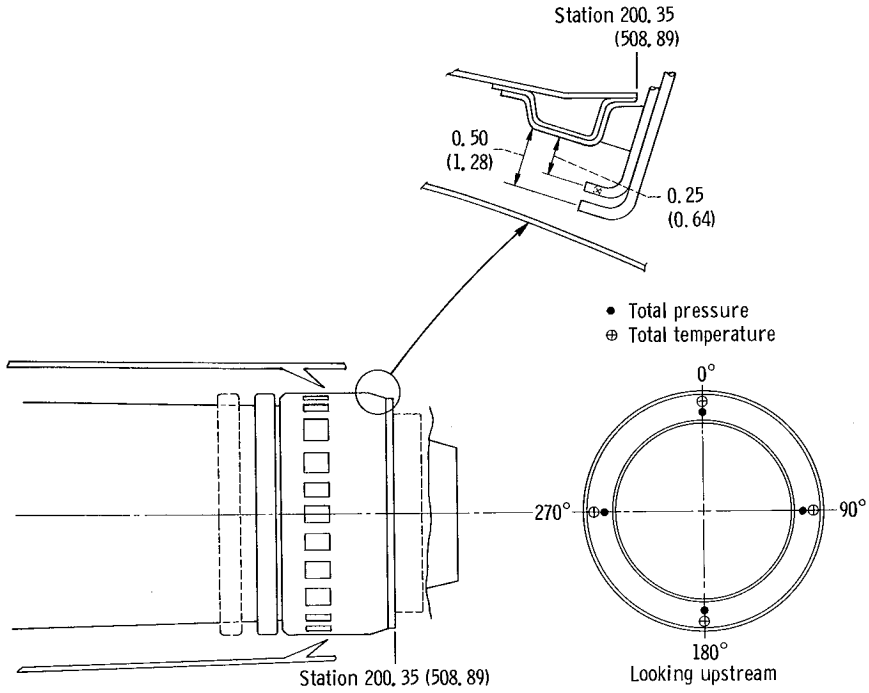

Figure 10. - Secondary passage instrumentation. (Dimensions are in inches (cm).)

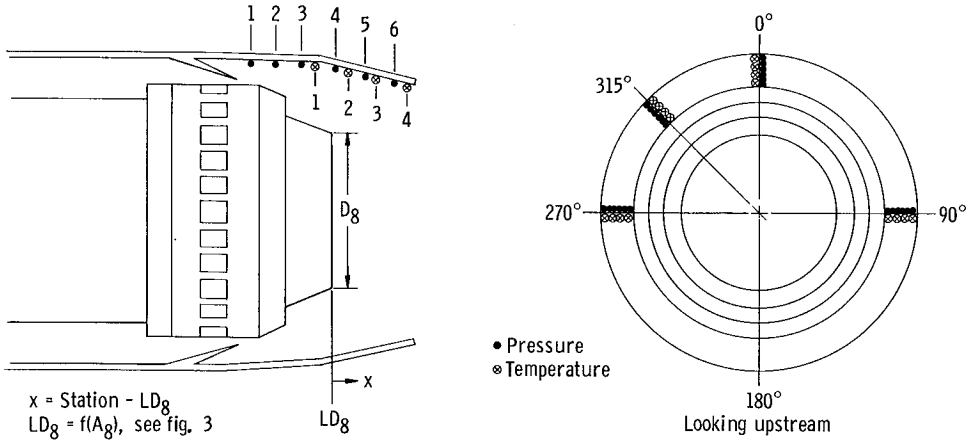

Instrumentation number	Door position, deg							
	16		20		8-16		10-20	
	Axial distance of instrumentation from compressor face, a							
	in.	cm	in.	cm	in.	cm	in.	cm
Door pressures								
1	193.23	490.80	193.23	490.80	193.46	491.39	193.46	491.39
2	194.74	494.64	194.74	494.64	195.45	496.44	195.42	496.37
3	196.59	499.34	196.59	499.34	197.42	501.45	197.41	501.42
4	198.76	504.85	198.76	504.85	199.37	506.4	199.32	506.27
5	200.93	510.36	200.83	510.11	201.3	511.30	201.19	511.02
6	203.09	515.85	202.96	515.52	202.22	513.64	199.13	515.80
Door temperatures								
1	198.54	504.29	198.38	503.89	198.54	504.29	198.38	503.86
2	200.42	509.07	200.26	508.66	200.42	509.07	200.26	508.66
3	202.3	513.84	202.14	513.44	202.3	513.84	202.14	513.44
4	204.18	518.62	204.02	518.21	204.18	518.62	204.02	518.21

Figure 11. - Auxilary inlet door instrumentation.

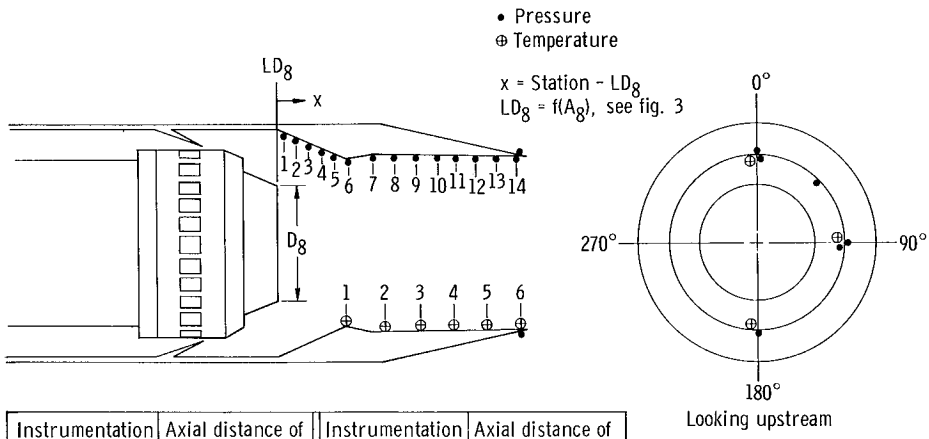

Instrumentation number	Axial distance of instrumentation from compressor face, a	
	in.	cm
Pressure		
1	205.13	521.03
2	206.17	523.67
3	207.87	527.99
4	209.57	532.31
5	211.27	536.63
6	212.97	540.94
7	215.6	547.5
8	218.1	554.0
9	220.7	560.5
10	223.2	567.0
11	225.79	573.51
12	228.35	580.01
13	230.91	586.51
14	233.47	593.01
Temperature		
1	212.97	540.94
2	217.07	551.36
3	221.17	561.77
4	225.27	572.19
5	229.4	582.6
6	233.47	593.01

(a) Takeoff and transonic ejector.

Figure 12. - Instrumentation details of ejectors.

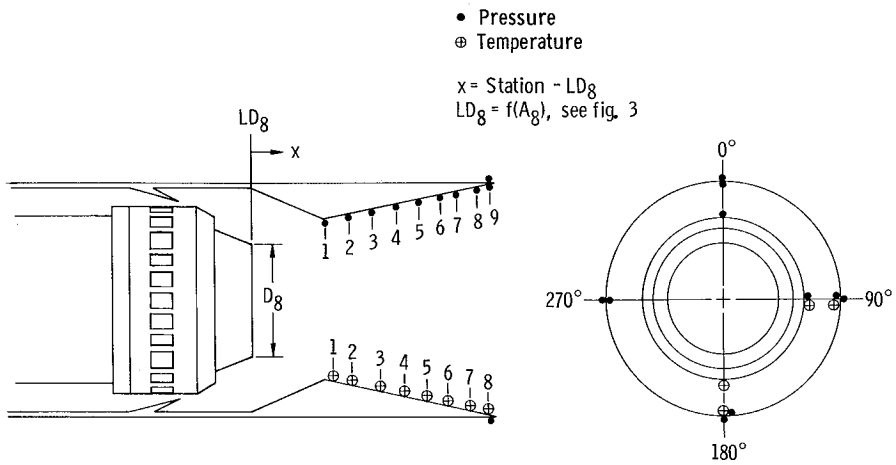

Instrumentation number	Axial distance of instrumentation from compressor face, a		Instrumentation number	Axial distance of instrumentation from compressor face, a	
	in.	cm		in.	cm
Pressure			Temperature		
1	213.08	541.22	1	212.90	540.77
2	214.85	545.72	2	213.90	543.31
3	218.08	553.93	3	215.90	548.39
4	221.31	562.13	4	217.8	553.21
5	224.46	570.13	5	221.7	563.12
6	227.28	577.29	6	225.6	573.02
7	230.13	584.53	7	228.6	580.64
8	232.88	591.52	8	233.4	592.84
9	233.87	594.02			

(b) Supersonic cruise ejector.

Figure 12. - Concluded.

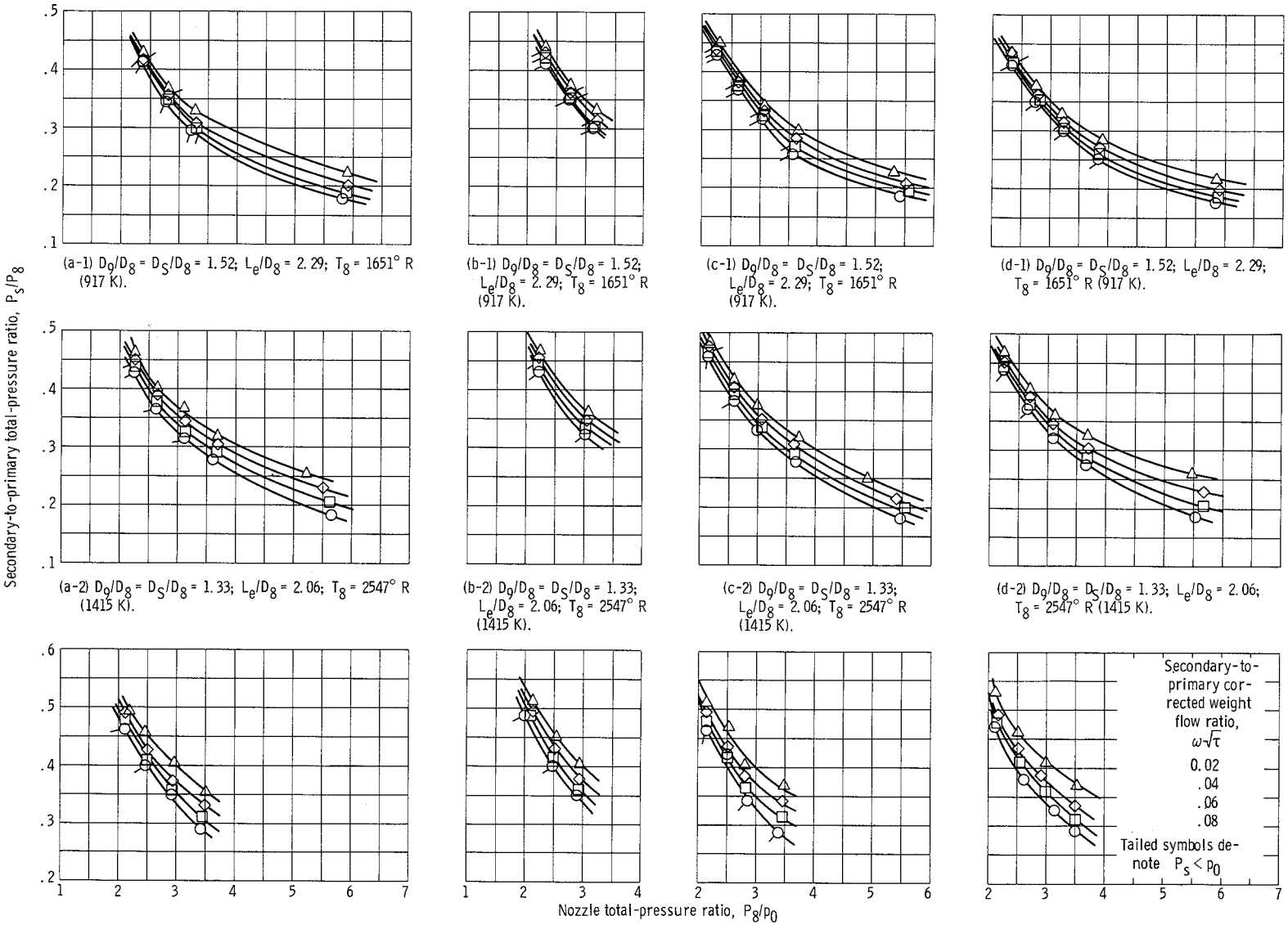

(a-1) $D_9/D_8 = D_S/D_8 = 1.52$; $L_e/D_8 = 2.29$; $T_8 = 1651°$ R (917 K).

(b-1) $D_9/D_8 = D_S/D_8 = 1.52$; $L_e/D_8 = 2.29$; $T_8 = 1651°$ R (917 K).

(c-1) $D_9/D_8 = D_S/D_8 = 1.52$; $L_e/D_8 = 2.29$; $T_8 = 1651°$ R (917 K).

(d-1) $D_9/D_8 = D_S/D_8 = 1.52$; $L_e/D_8 = 2.29$; $T_8 = 1651°$ R (917 K).

(a-2) $D_9/D_8 = D_S/D_8 = 1.33$; $L_e/D_8 = 2.06$; $T_8 = 2547°$ R (1415 K).

(b-2) $D_9/D_8 = D_S/D_8 = 1.33$; $L_e/D_8 = 2.06$; $T_8 = 2547°$ R (1415 K).

(c-2) $D_9/D_8 = D_S/D_8 = 1.33$; $L_e/D_8 = 2.06$; $T_8 = 2547°$ R (1415 K).

(d-2) $D_9/D_8 = D_S/D_8 = 1.33$; $L_e/D_8 = 2.06$; $T_8 = 2547°$ R (1415 K).

(a-3) $D_9/D_8 = D_S/D_8 = 1.18$; $L_e/D_8 = 1.88$; $T_8 = 3420°$ R (1900 K).

(b-3) $D_9/D_8 = D_S/D_8 = 1.18$; $L_e/D_8 = 1.88$; $T_8 = 3420°$ R (1900 K).

(c-3) $D_9/D_8 = D_S/D_8 = 1.18$; $L_e/D_8 = 1.88$; $T_8 = 3420°$ R (1900 K).

(d-3) $D_9/D_8 = D_S/D_8 = 1.18$; $L_e/D_8 = 1.88$; $T_8 = 3420°$ R (1900 K).

(a) 16° Open doors.

(b) 8°-16° Open doors.

(c) 20° Open doors.

(d) 10°-20° Open doors.

Figure 13. - Pumping characteristics of takeoff ejector configuration.

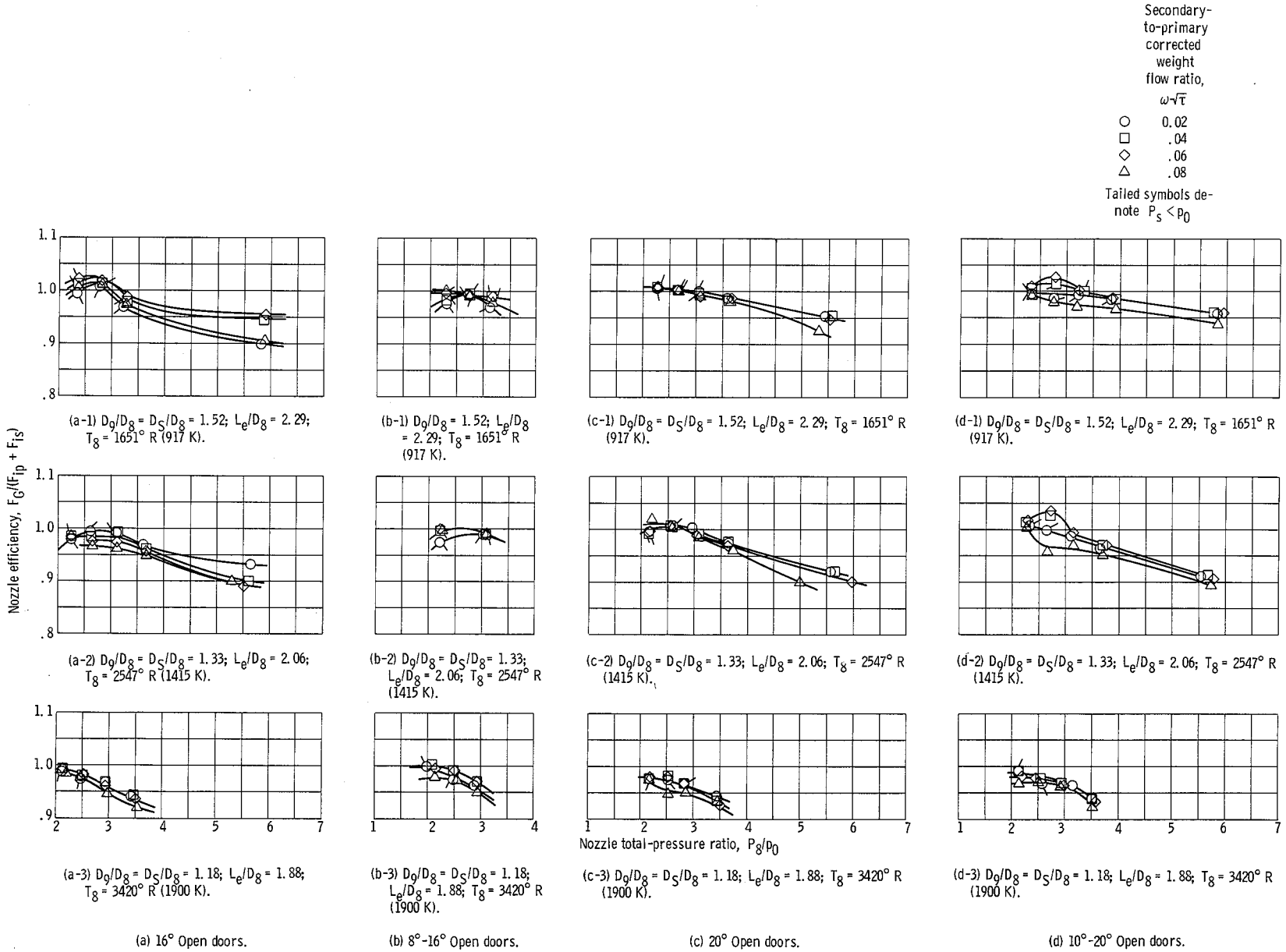

Figure 14. - Thrust characteristics of takeoff ejector configuration in terms of nozzle efficiency.

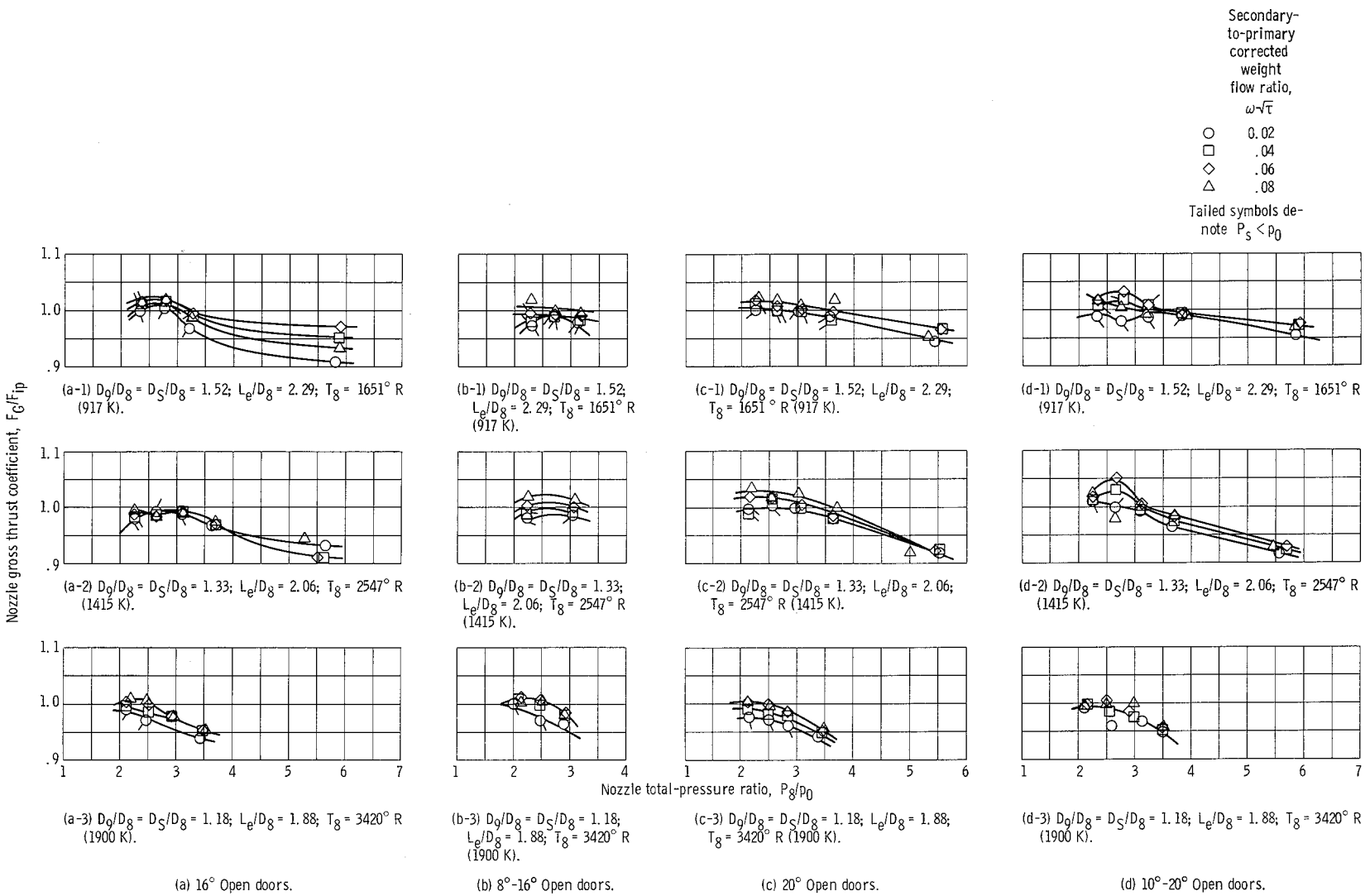

Figure 15. - Thrust characteristics of takeoff ejector configuration in terms of nozzle gross thrust coefficient.

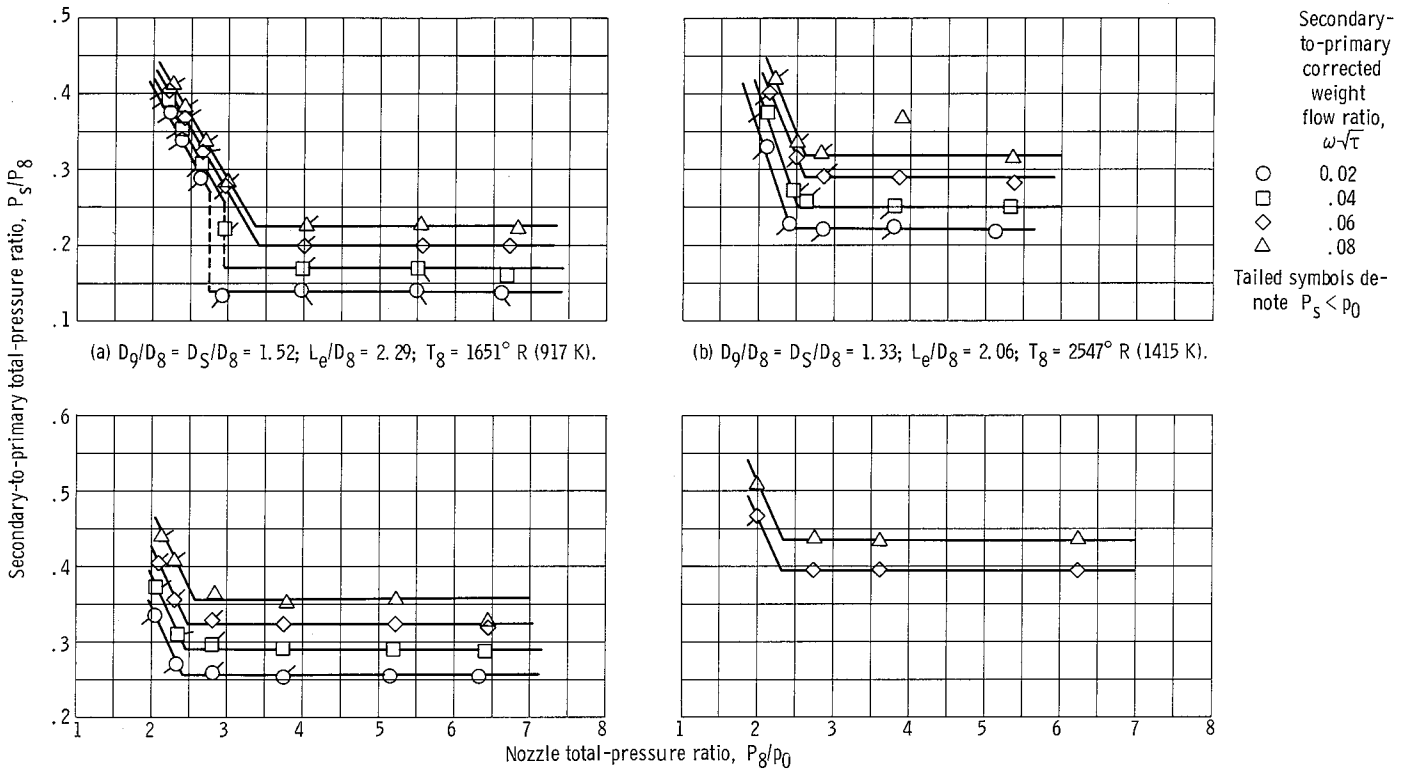

(a) $D_9/D_8 = D_s/D_8 = 1.52$; $L_e/D_8 = 2.29$; $T_8 = 1651°$ R (917 K).

(b) $D_9/D_8 = D_s/D_8 = 1.33$; $L_e/D_8 = 2.06$; $T_8 = 2547°$ R (1415 K).

(c) $D_9/D_8 = D_s/D_8 = 1.28$; $L_e/D_8 = 2.00$; $T_8 = 2970°$ R (1650 K).

(d) $D_9/D_8 = D_s/D_8 = 1.18$; $L_e/D_8 = 1.88$; $T_8 = 3420°$ R (1900 K).

Figure 16. - Pumping characteristics of transonic ejector configuration.

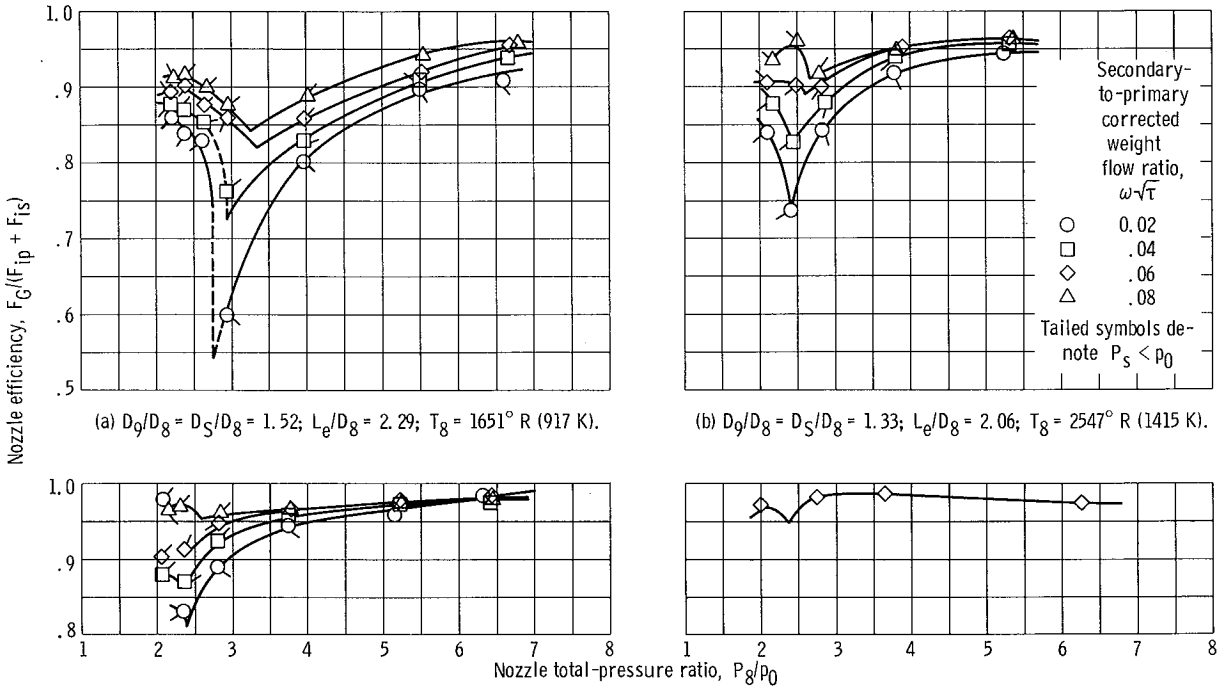

(a) $D_9/D_8 = D_S/D_8 = 1.52$; $L_e/D_8 = 2.29$; $T_8 = 1651°$ R (917 K).

(b) $D_9/D_8 = D_S/D_8 = 1.33$; $L_e/D_8 = 2.06$; $T_8 = 2547°$ R (1415 K).

(c) $D_9/D_8 = D_S/D_8 = 1.28$; $L_e/D_8 = 2.00$; $T_8 = 2970°$ R (1650 K).

(d) $D_9/D_8 = D_S/D_8 = 1.18$; $L_e/D_8 = 1.88$; $T_8 = 3420°$ R (1900 K).

Figure 17. - Thrust characteristics of transonic ejector configuration in terms of nozzle efficiency.

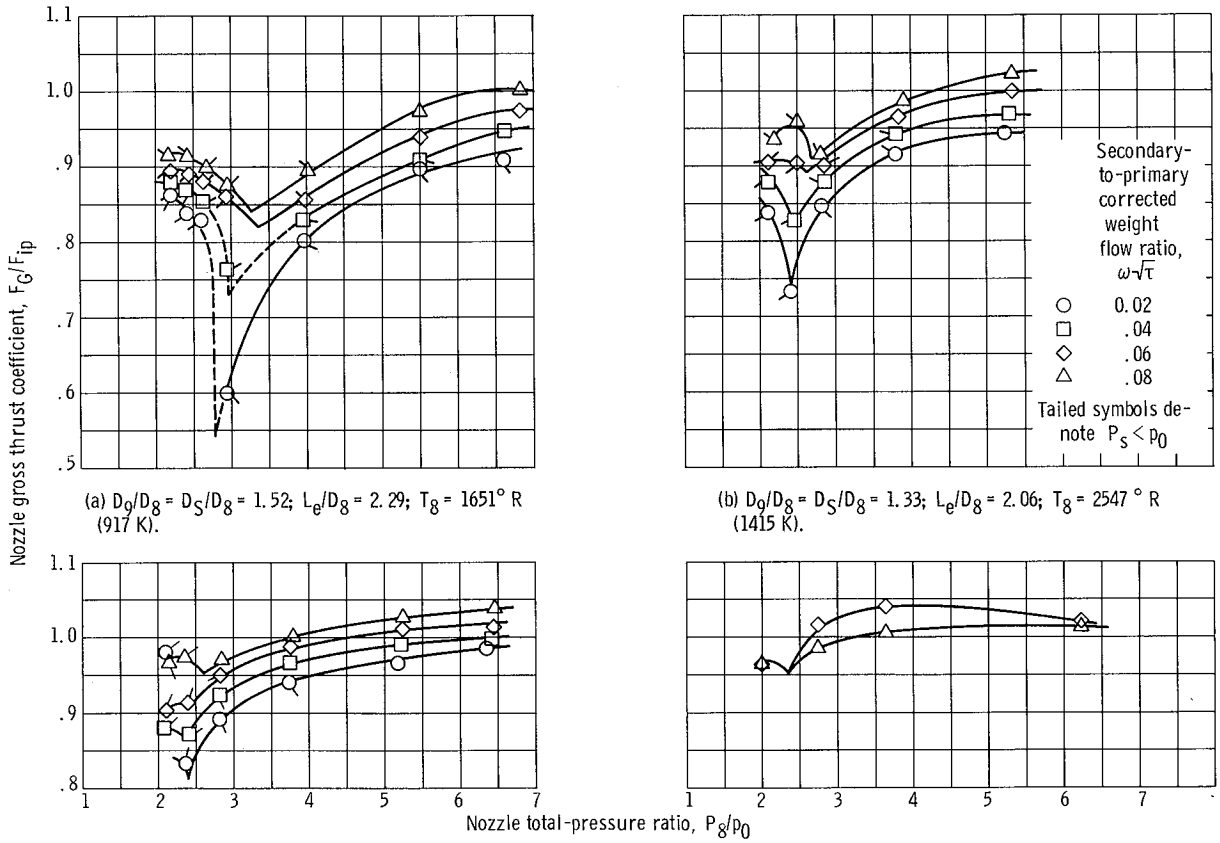

(a) $D_9/D_8 = D_S/D_8 = 1.52$; $L_e/D_8 = 2.29$; $T_8 = 1651°$ R (917 K).

(b) $D_9/D_8 = D_S/D_8 = 1.33$; $L_e/D_8 = 2.06$; $T_8 = 2547°$ R (1415 K).

(c) $D_9/D_8 = D_S/D_8 = 1.28$; $L_e/D_8 = 2.00$; $T_8 = 2970°$ R (1650 K).

(d) $D_9/D_8 = D_S/D_8 = 1.18$; $L_e/D_8 = 1.88$; $T_8 = 3420°$ R (1900 K).

Figure 18. - Thrust characteristics of transonic ejector configuration in terms of nozzle gross thrust coefficient.

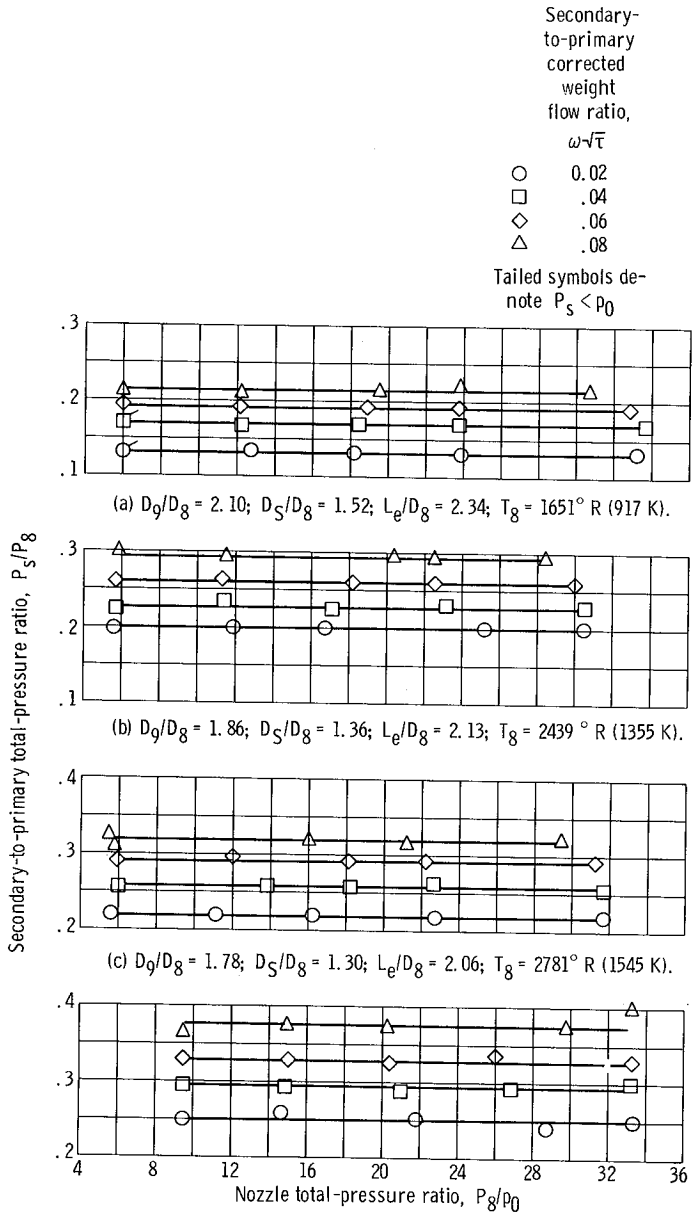

(a) $D_9/D_8 = 2.10$; $D_s/D_8 = 1.52$; $L_e/D_8 = 2.34$; $T_8 = 1651°$ R (917 K).

(b) $D_9/D_8 = 1.86$; $D_s/D_8 = 1.36$; $L_e/D_8 = 2.13$; $T_8 = 2439°$ R (1355 K).

(c) $D_9/D_8 = 1.78$; $D_s/D_8 = 1.30$; $L_e/D_8 = 2.06$; $T_8 = 2781°$ R (1545 K).

(d) $D_9/D_8 = 1.72$; $D_s/D_8 = 1.25$; $L_e/D_8 = 2.01$; $T_8 = 3105°$ R (1725 K).

Figure 19. - Pumping characteristics of supersonic cruise ejector configuration.

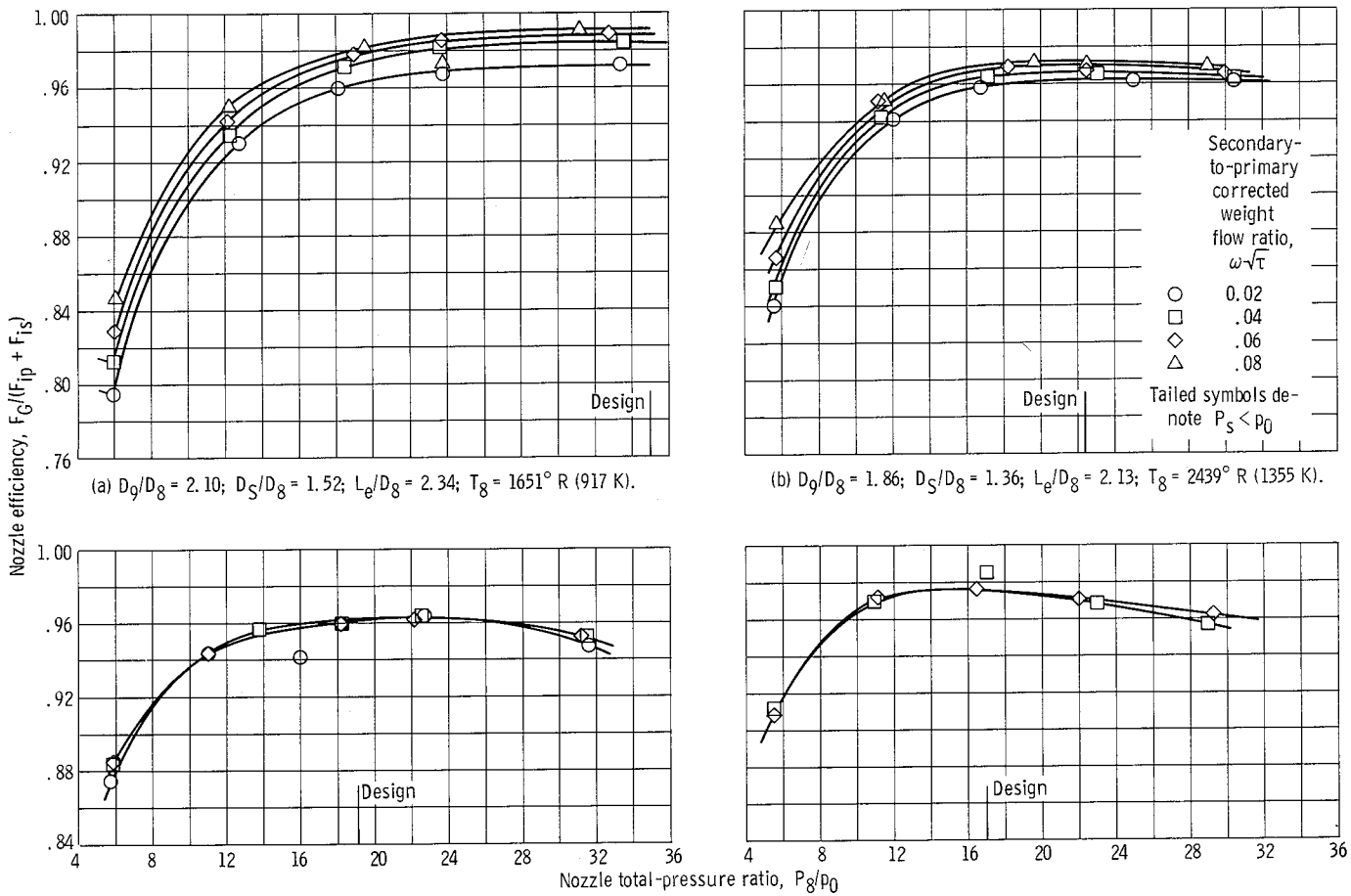

(a) $D_9/D_8 = 2.10$; $D_S/D_8 = 1.52$; $L_e/D_8 = 2.34$; $T_8 = 1651°$ R (917 K).

(b) $D_9/D_8 = 1.86$; $D_S/D_8 = 1.36$; $L_e/D_8 = 2.13$; $T_8 = 2439°$ R (1355 K).

(c) $D_9/D_8 = 1.78$; $D_S/D_8 = 1.30$; $L_e/D_8 = 2.06$; $T_8 = 2781°$ R (1545 K).

(d) $D_9/D_8 = 1.72$; $D_S/D_8 = 1.25$; $L_e/D_8 = 2.01$; $T_8 = 3105°$ R (1725 K).

Figure 20. - Thrust characteristics of supersonic cruise ejector configuration in terms of nozzle efficiency.

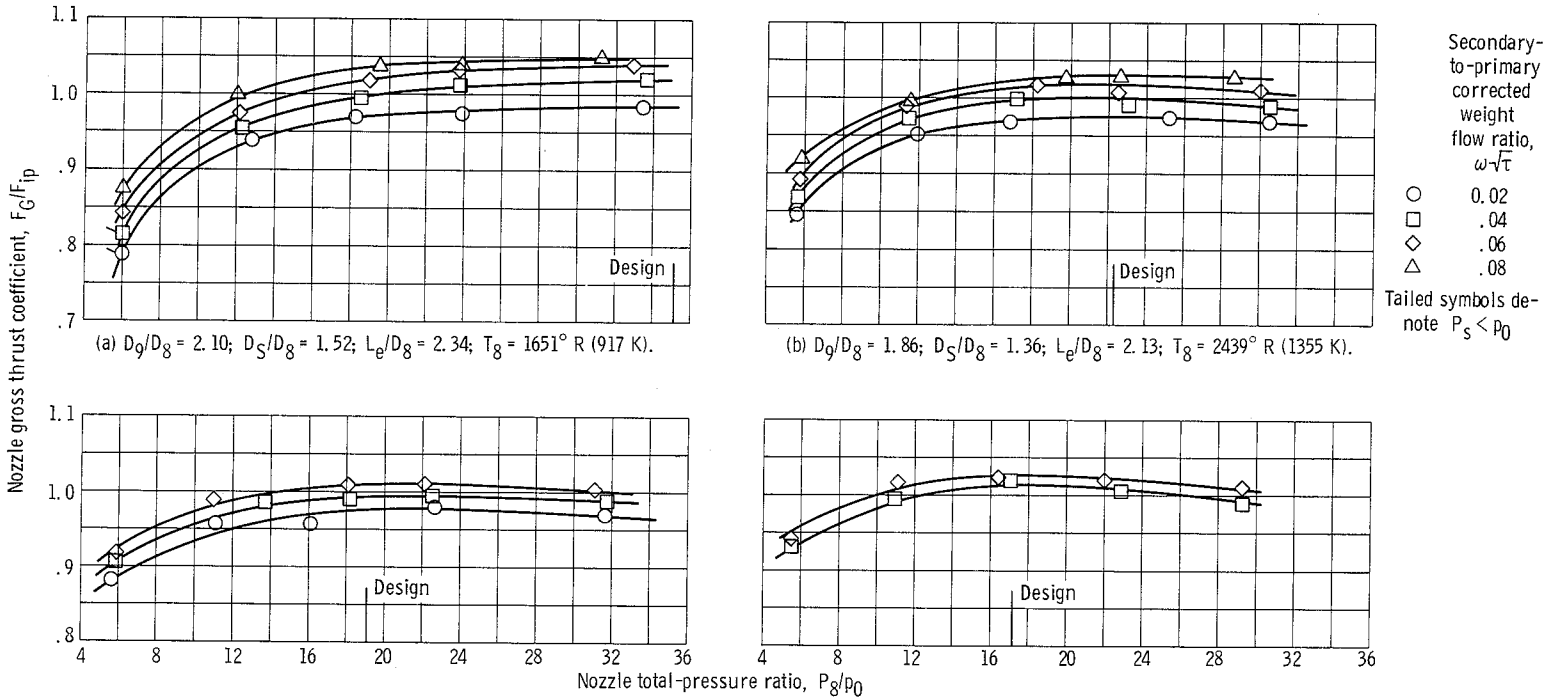

(a) D_9/D_8 = 2.10; D_S/D_8 = 1.52; L_e/D_8 = 2.34; T_8 = 1651° R (917 K).

(b) D_9/D_8 = 1.86; D_S/D_8 = 1.36; L_e/D_8 = 2.13; T_8 = 2439° R (1355 K).

(c) D_9/D_8 = 1.78; D_S/D_8 = 1.30; L_e/D_8 = 2.06; T_8 = 2781° R (1545 K).

(d) D_9/D_8 = 1.72; D_S/D_8 = 1.25; L_e/D_8 = 2.01; T_8 = 3105° R (1725 K).

Figure 21. - Thrust characteristics of supersonic ejector configuration in terms of nozzle gross thrust coefficient.

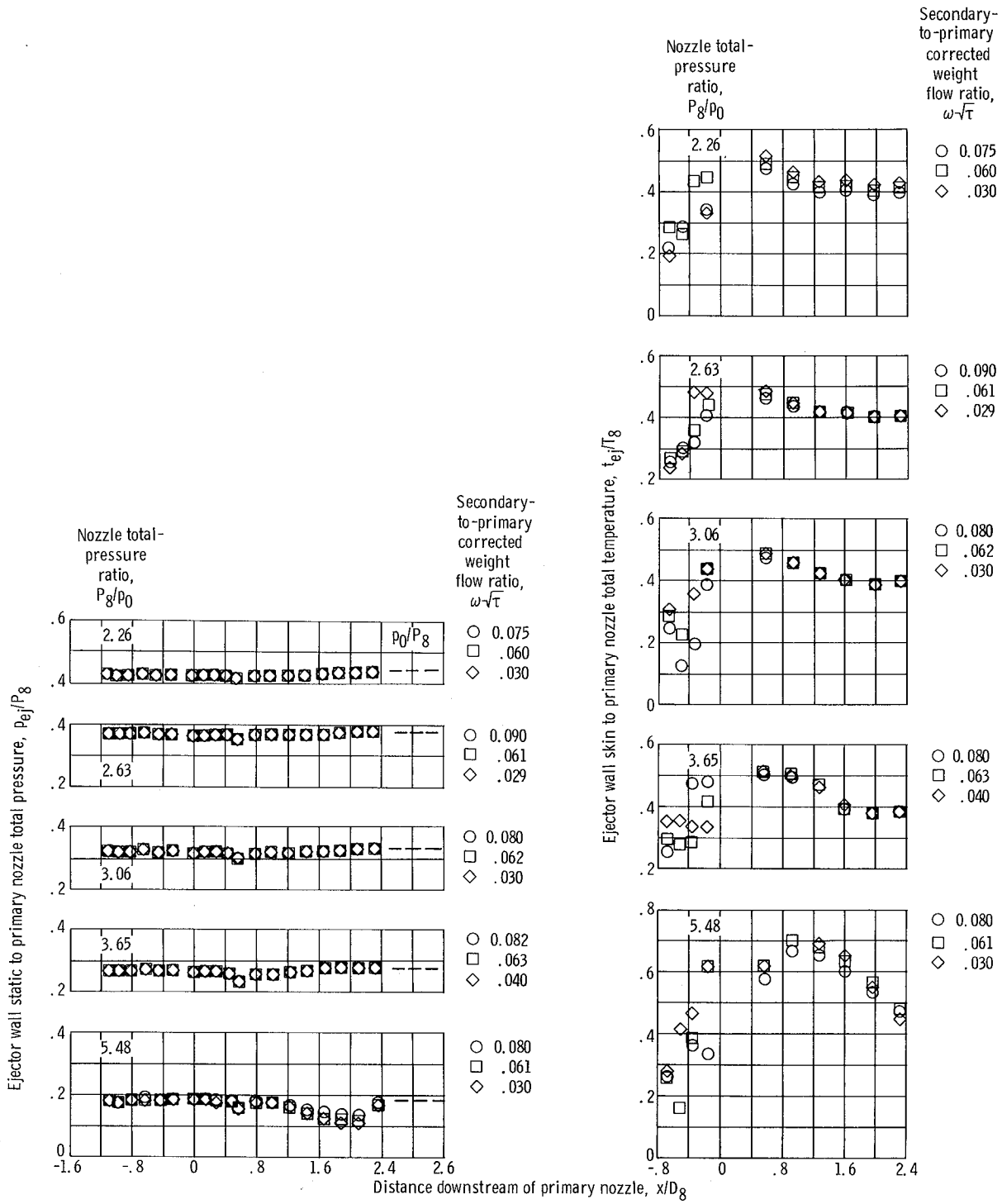

(a-1) Pressure distribution: $D_9/D_8 = D_S/D_8 = 1.52$; $P_8 = 19.44$ psia (134.1 kN/m^2).

(a-2) Temperature distribution: $D_9/D_8 = D_S/D_8 = 1.52$; $T_8 = 1651^\circ$ R (917 K).

(a) 20° Open doors.

Figure 22. - Wall pressure and temperature distributions of takeoff ejector configuration.

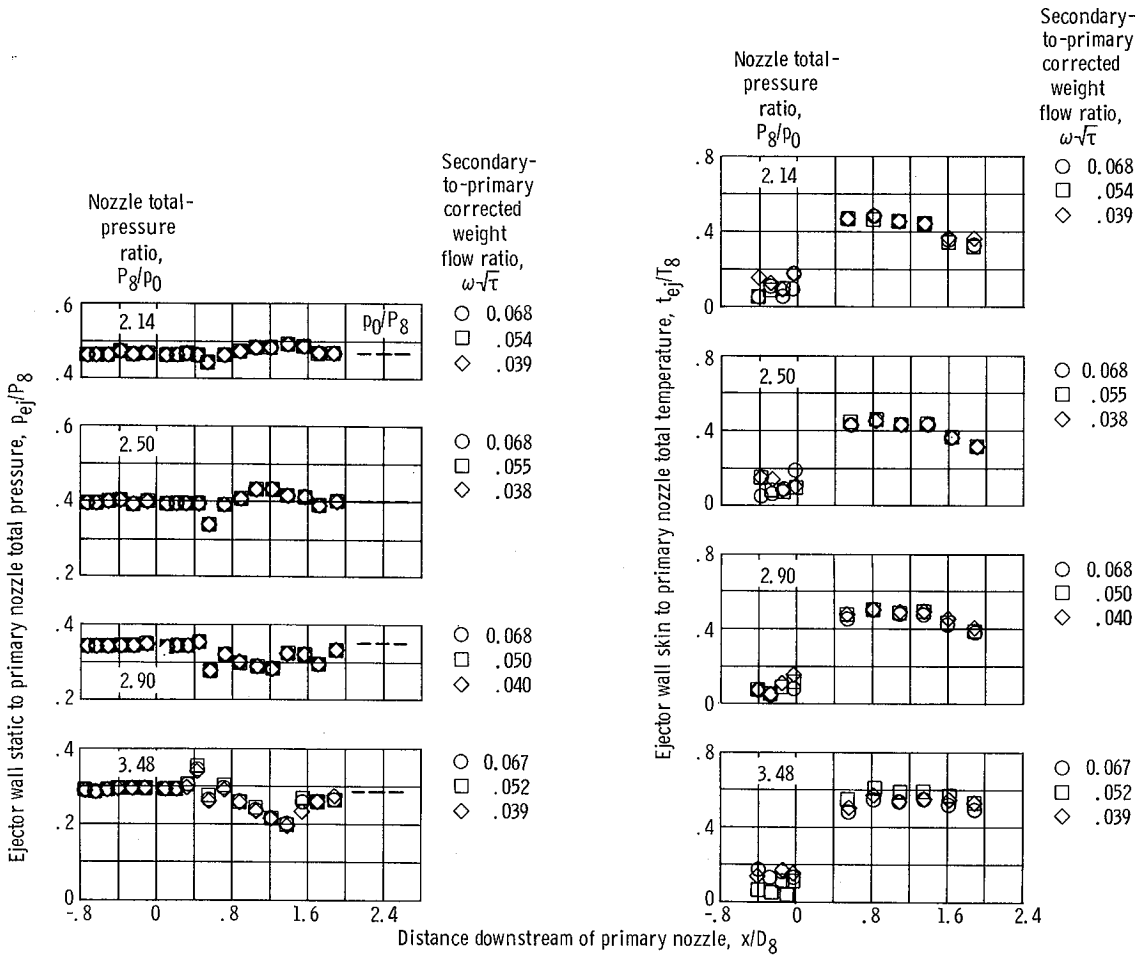

(a-3) Pressure distribution: $D_9/D_8 = D_S/D_8 = 1.18$; $P_8 = 18.01$ psia (124.2 kN/m^2).

(a-4) Temperature distribution: $D_9/D_8 = D_S/D_8 = 1.18$; $T_8 = 3420°$ R (1900 K).

Figure 22. - Continued.

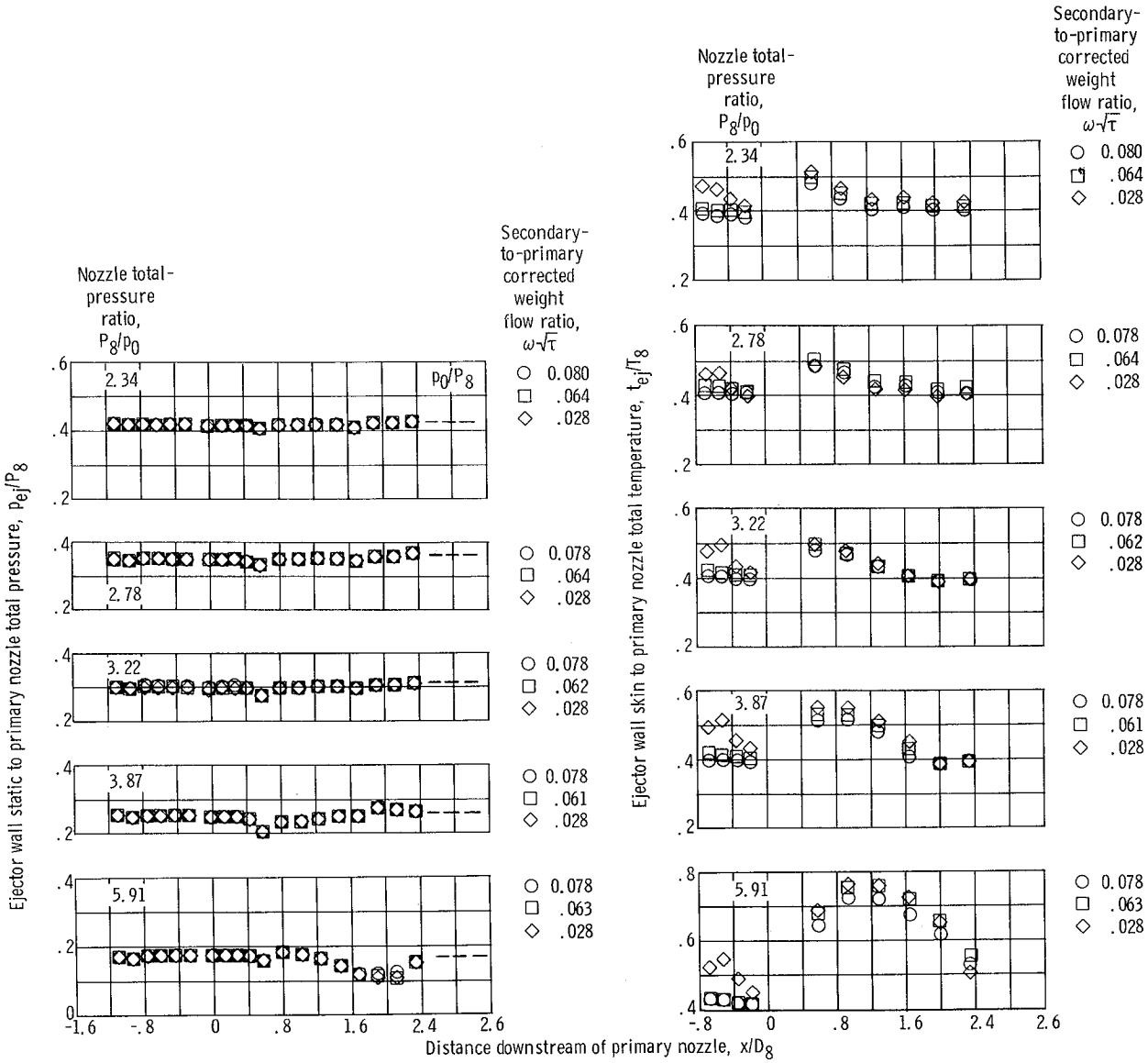

(b-1) Pressure distribution: $D_9/D_8 = D_S/D_8 = 1.52$; $P_8 = 19.44$ psia (134.1 kN/m^2).

(b-2) Temperature distribution: $D_9/D_8 = D_S/D_8 = 1.52$; $T_8 = 1651°$ R (917 K).

(b) 10°-20° Open doors.

Figure 22. - Continued.

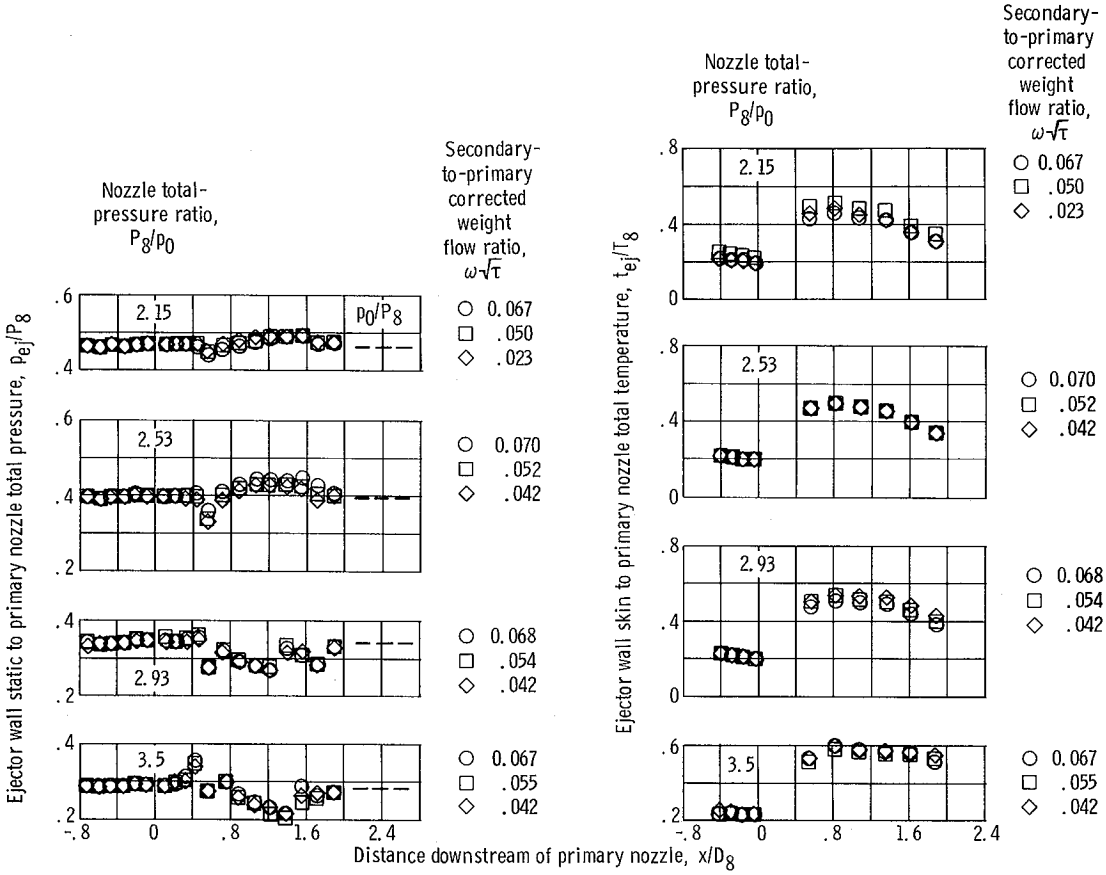

(b-3) Pressure distribution; $D_9/D_8 = D_S/D_8 = 1.18$; $P_8 = 18.01$ psia (124.2 kN/m^2).

(b-4) Temperature distribution: $D_9/D_8 = D_S/D_8 = 1.18$; $T_8 = 3420°$ R (1900 K).

Figure 22. - Concluded.

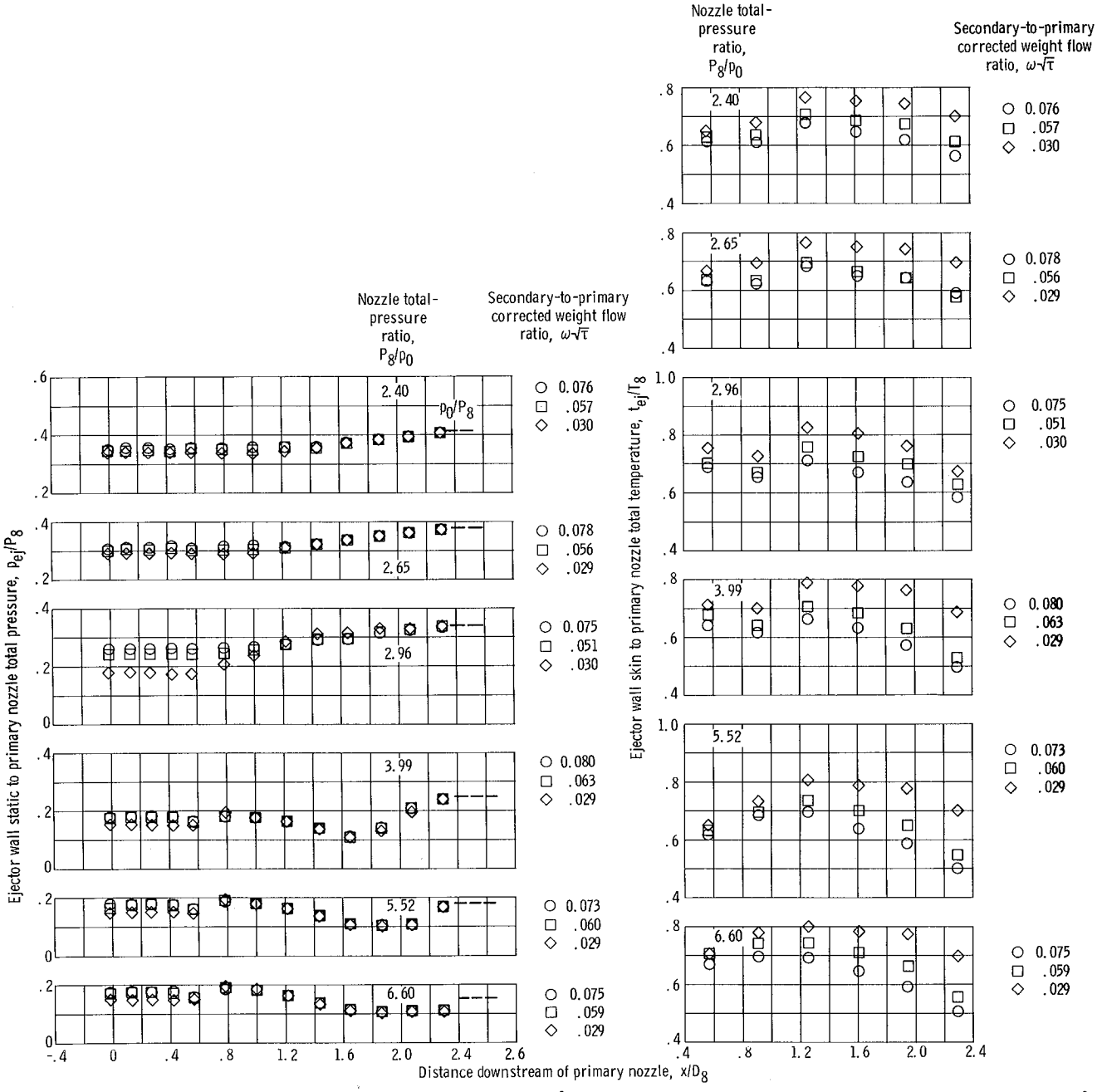

(a) Pressure distribution: $D_9/D_8 = D_S/D_8 = 1.52$; $P_8 = 19.44$ psia (134.1 kN/m^2).

(b) Temperature distribution: $D_9/D_8 = D_S/D_8 = 1.52$; $T_8 = 1651°$ R (917 K).

Figure 23. - Wall pressure and temperature distributions of transonic ejector configuration.

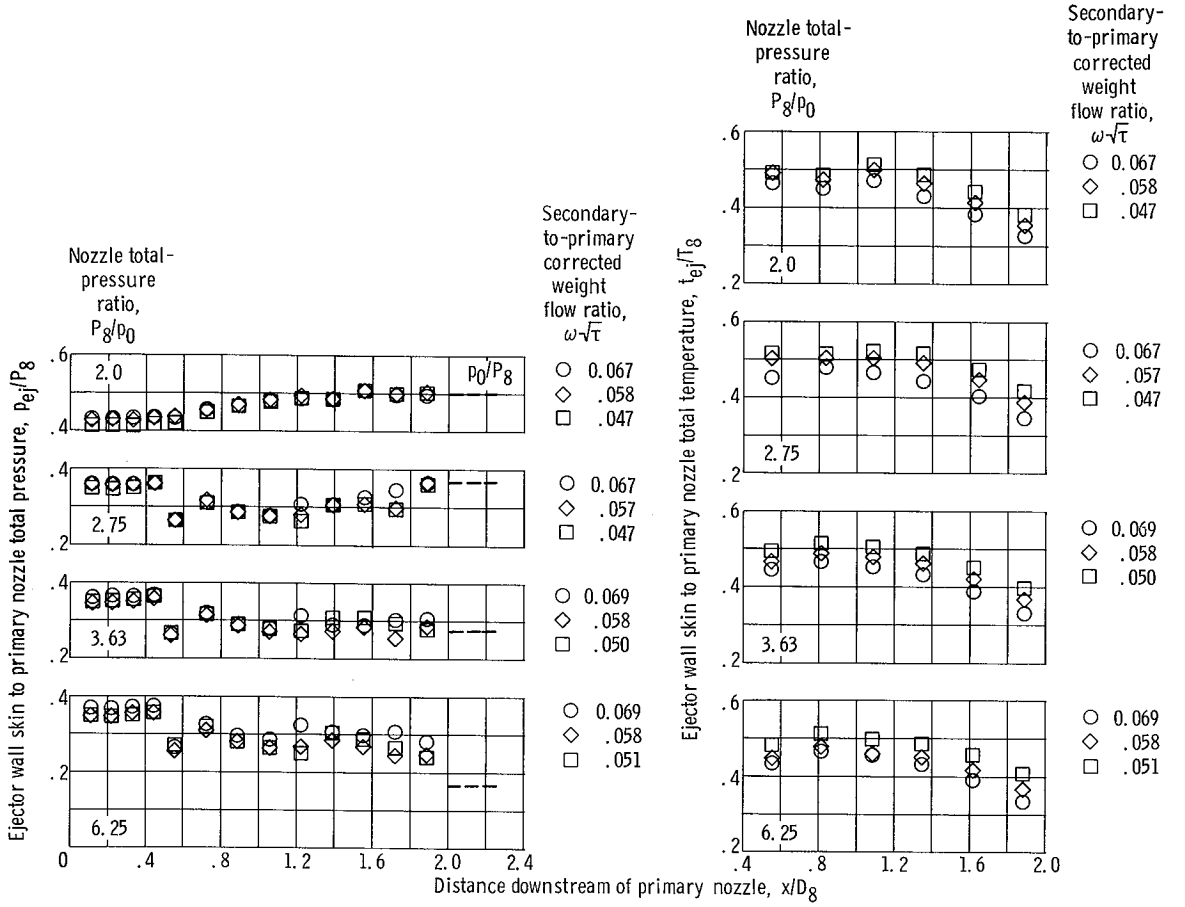

(c) Pressure distribution: $D_9/D_8 = D_S/D_8 = 1.18$; $P_8 = 18.01$ psia (124.2 kN/m^2).

(d) Temperature distribution: $D_9/D_8 = D_S/D_8 = 1.18$; $T_8 = 3420°$ R (1900 K).

Figure 23. - Concluded.

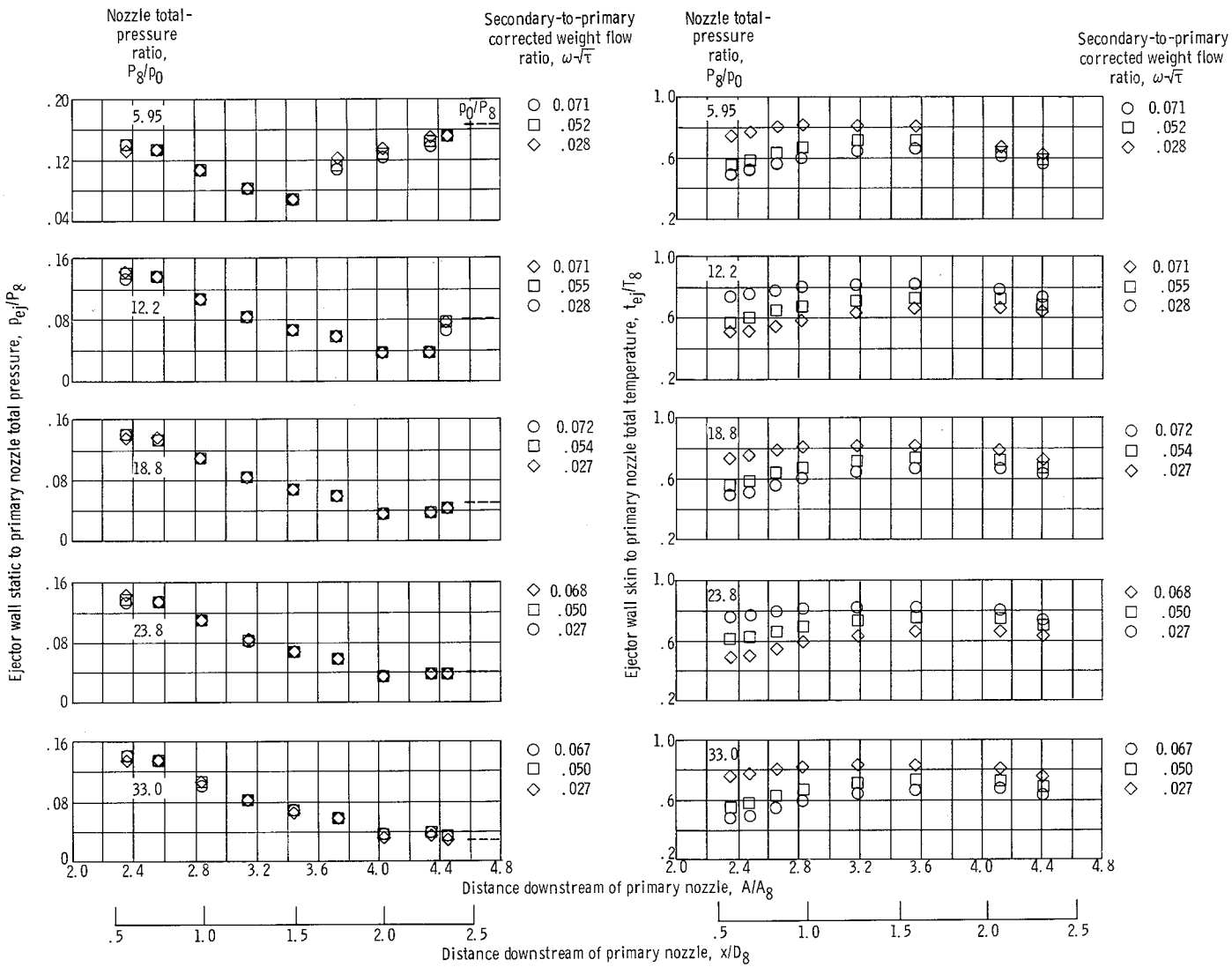

(a) Pressure distribution: $D_9/D_8 = 2.1$; $D_S/D_8 = 1.52$; $P_8 = 32.07$ psia (221.2 kN/m^2).

(b) Temperature distribution: $D_9/D_8 = 2.1$; $D_S/D_8 = 1.52$; $T_8 = 1651^\circ$ R (917 K).

Figure 24. - Wall pressure and temperature distributions of supersonic cruise configuration.

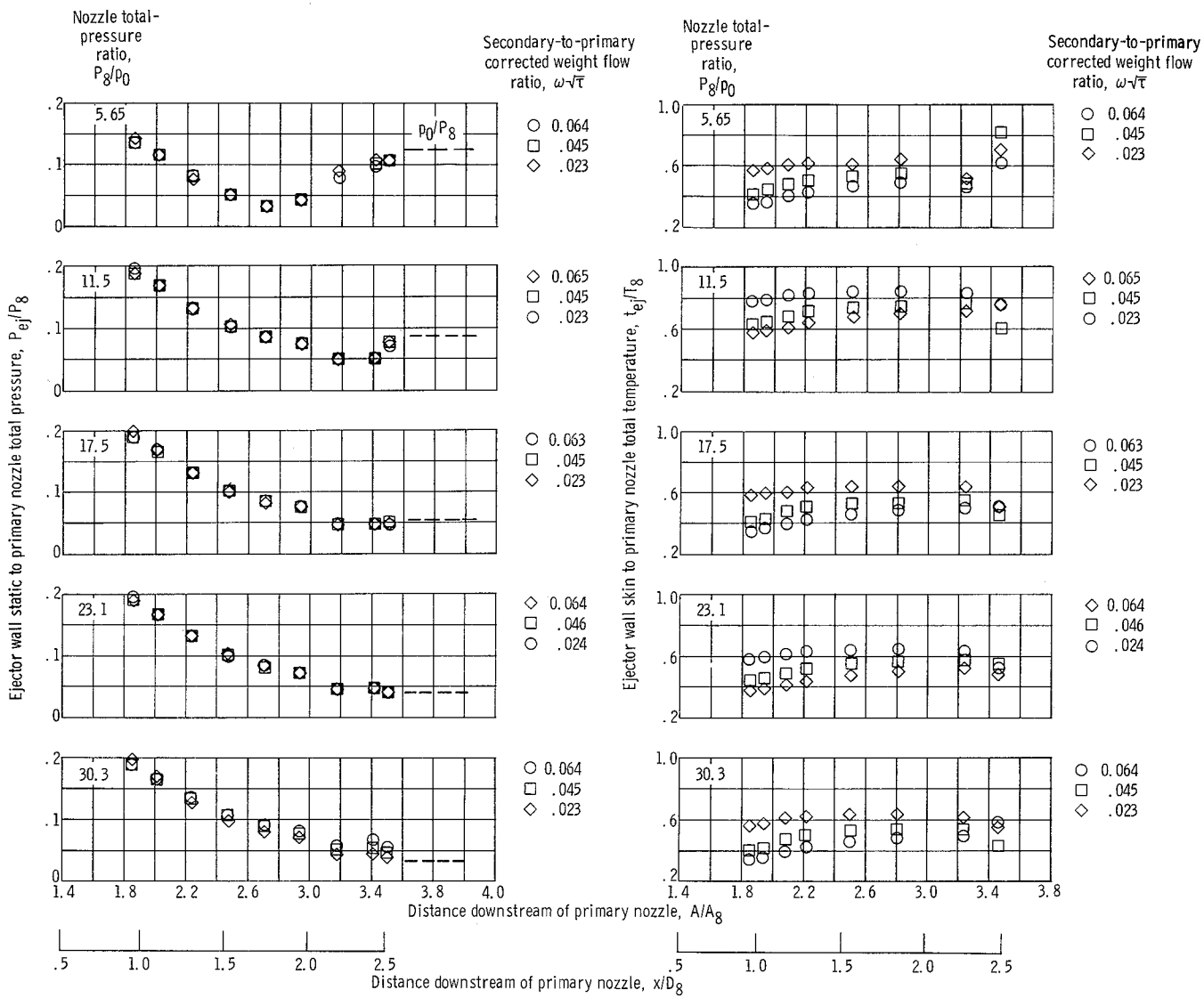

(c) Pressure distribution: $D_9/D_8 = 1.86$; $D_S/D_8 = 1.36$; $P_8 = 30.10$ psia (207.5 kN/m^2).

(d) Temperature distribution: $D_9/D_8 = 1.86$; $D_S/D_8 = 1.36$; $T_8 = 2439°$ R (1355 K).

Figure 24. - Continued.

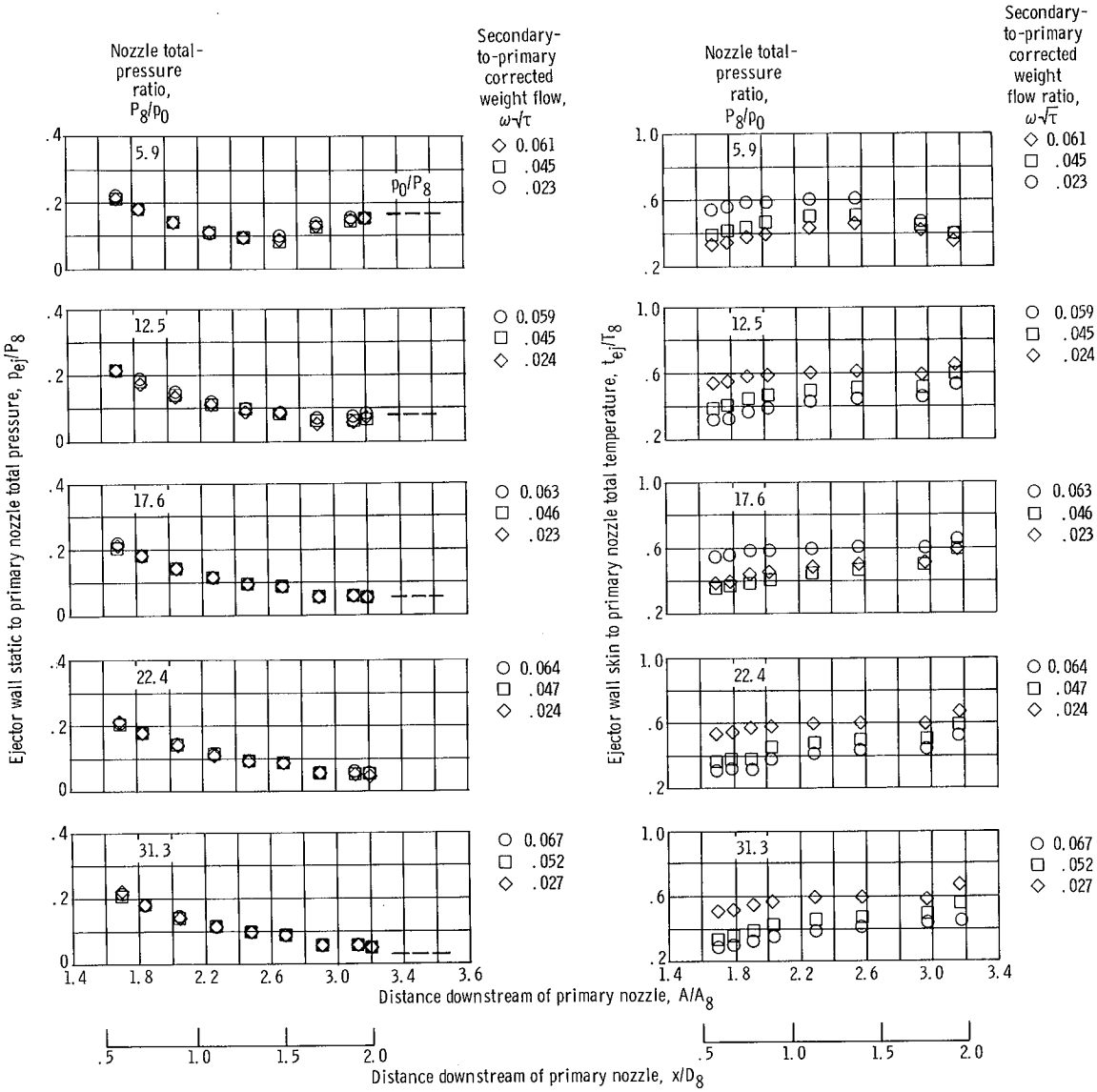

(e) Pressure distribution: $D_9/D_8 = 1.78$; $D_S/D_8 = 1.30$; $P_8 = 30.72$ psia (211.8 kN/m^2).

(f) Temperature distribution: $D_9/D_8 = 1.78$; $D_S/D_8 = 1.30$; $T_8 = 2781°$ R (1545 K).

Figure 24. - Continued.

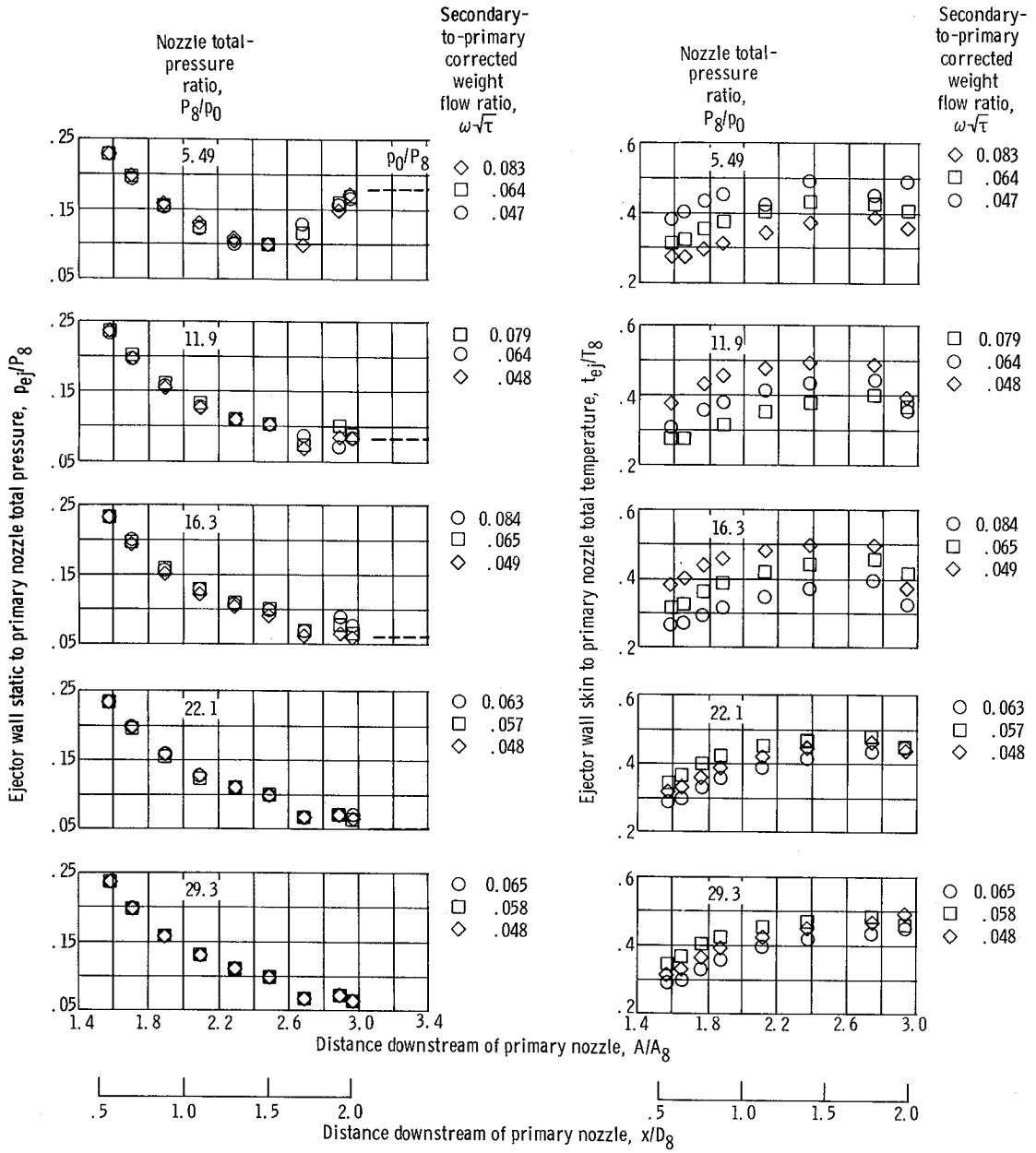

(g) Pressure distribution: $D_9/D_8 = 1.72$; D_S/D $P_8 = 29.62$ psia (204.3 kN/m^2).

(h) Temperature distribution: $D_9/D_8 = 1.72$; $D_S/D_8 = 1.25$; $T_8 = 3105°$ R (1725 K).

Figure 24. - Concluded.

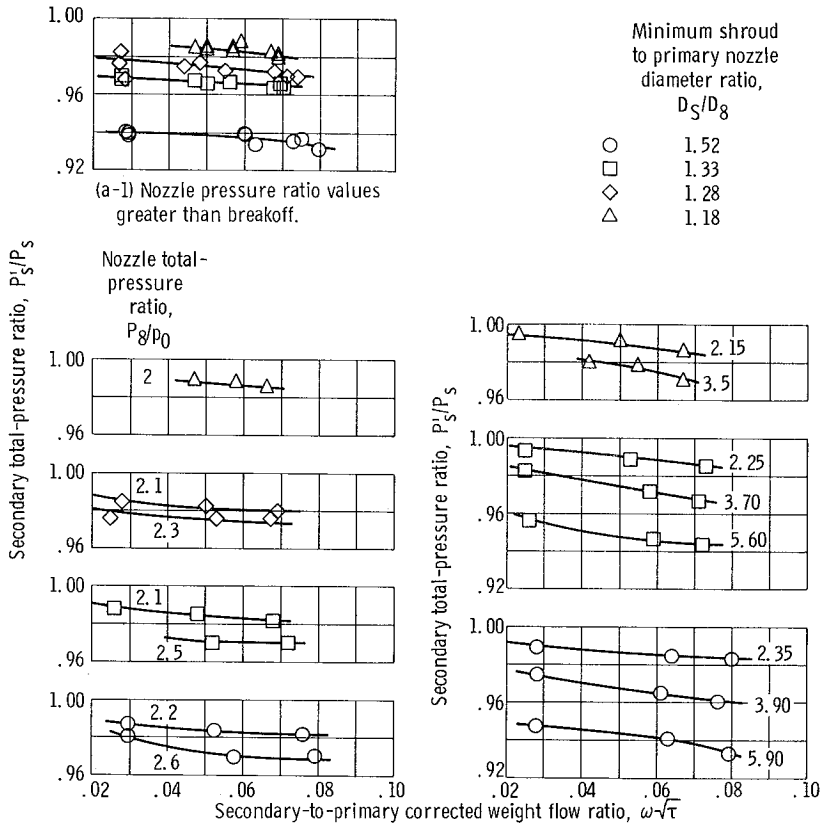

(a-1) Nozzle pressure ratio values greater than breakoff.

(a-2) Nozzle pressure ratio values less than breakoff.

(a) Transonic ejector configuration.

(b) Takeoff ejector configuration; 10°-20° open doors.

Figure 25. - Total-pressure loss through secondary-flow passage.

NASA-Langley, 1970 — 28 E-5459